# COMPARISON OF NUMERICAL METHODS FOR SOLUTION OF THE CONVECTION-DIFFUSION EQUATION IN ONE AND TWO DIMENSIONS

by

Christine Ehlig

Submitted to the Department of Chemical and Petroleum Engineering and the Faculty of the Graduate School of the University of Kansas in partial fulfillment of the requirements for the degree of Master of Science

Thesis Committee

_____

Chairman

_____

_____

To my husband

ACKNOWLEDGEMENTS

The author wishes to express special thanks to Dr. Lois Mansfield for her advice on the initial statement of the objectives for this study, to Dr. Carl McElwee for his useful suggestions throughout the project, and to Dr. Don Green for helping to bring the thesis to completion.

The author wishes to thank the Kansas Geological Survey for helping to prepare this thesis and the publication of a portion of the results, for providing me the chance to present my results in a professional meeting, and for offering me a beneficial position as a research assistant.

The author also wishes to thank the Department of Chemical and Petroleum Engineering for providing a flexible and useful plan of study.

ABSTRACT

Numerical simulations of miscible displacement in porous media require solution of the convection-diffusion equations. Numerical solutions of convection-diffusion equations exhibit two types of errors: oscillations about the correct solution and numerical dispersion. A number of numerical methods involving either finite difference or finite element techniques have been proposed. In this work five numerical methods for solving the one-dimensional convection-diffusion equation are examined. Finite element routines using chapeau and cubic Hermite basis functions are compared to a central difference routine, a non-central difference routine, and a method which combines finite element and finite difference techniques by replacing the matrix multiplying the time derivative in the finite element procedure by the identity matrix (lumping). Although the finite element routines are clearly more accurate than the finite difference methods used here, all of the techniques suffer from the two previously mentioned types of errors.

In the literature bounds are given for the spacing and time step sizes which prevent oscillations. However, the number of nodes required to avoid oscillations in the solution is prohibitive. In this work, maximum node spacing, and time step sizes are determined through numerical experiments as a function of the Peclet number and the accuracy required of the solution. The finite element methods are shown to require fewer nodes than the finite difference methods for a given accuracy.

The finite element method using chapeau functions is extended to two dimensions through the use of cross-products of the basis functions over a square grid. A constant dispersion coefficient and steady state velocities are assumed. The flow system consisting of a point sink superimposed on a constant unidirectional velocity field is examined. Velocities for the well point and its nearest neighboring points are evaluated at a finite radius from the well to achieve mass balance over the grid block surrounding the well point. Results from the model are used to attempt to generalize the limits on the spacing and time step sizes for the one-dimensional case to two dimensions.

TABLE OF CONTENTS

# CHAPTER I

## INTRODUCTION

Numerical solutions of the convection-diffusion equations have received considerable attention in both the petroleum engineering and the groundwater literature. Their use in a variety of applications involving heat or mass transfer justifies this ongoing study. A number of numerical techniques for solving the one-dimensional convection-diffusion equation have been proposed. Some of these methods have been extended to higher dimensions. In general, however, extension to two or three dimensions proves to be fairly difficult. Choice of appropriate boundary and initial conditions for two- and three-dimensional models depends upon the particular application. In this work, the application of primary interest is groundwater quality modeling in two dimensions.

Finite difference models of the one-dimensional convection-diffusion equation exhibit two major difficulties: oscillations about the correct solution and numerical dispersion. Both the space and time discretizations contribute to these numerical errors. Finite element methods have been applied in an attempt to diminish or remove these difficulties.

Unfortunately, no method yet developed is completely free from the above numerical errors. However, with suitable choice of the node spacing and time step size, the numerical errors can be controlled. Hence, it is important to determine for a given method bounds on the node spacing and time step sizes which limit the errors to within a specified tolerance.

With this objective in mind, five numerical methods for solving the one-dimensional convection-diffusion equation are compared in this work. Finite element routines using chapeau and cubic Hermite basis functions are compared with a central difference routine, a non-central difference routine, and a finite element-finite difference combination. In the latter "combination" technique, the matrix which multiplies the time derivative in the chapeau function routine is replaced with the identity matrix (lumping). All of the methods compared in this work use equal node spacing and the Crank-Nicholson time discretization.

Bounds on the space and time step sizes which prevent oscillations in the central difference routine are provided in the literature (29). These bounds appear to apply to the finite element routines as well. Unfortunately, the number of nodes required using these criteria is prohibitive for many practical problems. However, if small oscillations (10%) are tolerated, the finite element method requires far fewer modes than the finite difference method and can compute equally accurate solutions in fewer time steps. In this work, the maximum node space and time step values are determined as a function of the Peclet number and the specified accuracy for the central difference method and the two finite element methods.

The final objective of this work is to attempt to extend the bounds on the node spacing and time step determined for the one-dimensional equation to the two-dimensional convection-diffusion equation. The model chosen to be tested is a finite element model using cross-products of chapeau functions on a square grid. Fairly simple flow geometries are modeled using steady state analytical solutions for the velocity vectors. The dispersion coefficient is assumed to be constant.

Results for the two-dimensional model were less definitive. The number of parameters and the complexity of the model for even simple geometries make generalizations about the maximum space and time step sizes difficult to determine.

# CHAPTER II

# THEORY

Miscible displacement in porous media is governed chiefly by three types of transport processes: molecular diffusion, hydrodynamic dispersion, and convective transport. The molecular diffusion flux, F, when considered on a macroscopic scale which is large compared to the individual grains of the porous matrix, is described by the usual Fick's law equation, $F = -\frac{D}{\tau}\frac{dC}{dx}$, where the ordinary molecular diffusivity D is divided by a tortuosity factor, $\tau$, which reflects the "crookedness" of the path through the void spaces in the porous medium. Discussions of the molecular diffusion process are found in Blackman (3), Brigham, Reed, and Dew (6), and Perkins and Johnston (25). Hydrodynamic dispersion in multi-dimensional flow is a complex phenomena best described by a dispersion tensor. Detailed mathematical analyses of the dispersion process are found in Scheidegger (32, 33) Fara and Scheidegger (11), Bear (2), Bachmat and Bear (1), and de Josselin de Jong (10). Convective transport results from the bulk movement of the fluids through the porous medium according to Darcy's Law.

## II.A Differential Equations Used to Represent Miscible Displacement in a Porous Medium.

The equations describing multi-dimensional, incompressible, miscible displacement in a porous medium are summarized in Settari, Price, and Dupont (34). The two-dimensional convection-diffusion equation is given by

$$\frac{\partial}{\partial x}\left(D_x\frac{\partial C}{\partial x} - u_x C\right) + \frac{\partial}{\partial y}\left(D_y\frac{\partial C}{\partial y} - u_y C\right) = \Phi\frac{\partial C}{\partial t} + qC_i \qquad \text{(II.A.1)}$$

where dispersion coefficients $D_x$ and $D_y$ are given by

$$D_x = \Phi D/\tau + \alpha_\ell\frac{u_x^2}{|u|} + \alpha_t\frac{u_y^2}{|u|}$$
$$D_y = \Phi D/\tau + \alpha_\ell\frac{u_y^2}{|u|} + \alpha_t\frac{u_x^2}{|u|} \qquad \text{(II.A.2)}$$

and the Darcy velocity vectors $\vec{u}(x,y) = (u_x, u_y)$ are determined from the continuity equation for incompressible flow through porous media,

$$\frac{\partial u_x}{\partial x} + \frac{\partial u_y}{\partial y} = -q \qquad \text{(II.A.3)}$$

$$\text{where } u_x = \frac{-k_x}{\mu}\frac{\partial h}{\partial x}, \quad u_y = \frac{-k_y}{\mu}\frac{\partial h}{\partial y}$$
$$\text{and } h = \frac{p}{\rho g} + z \qquad \text{(II.A.4)}$$

$C(x,y,t)$ = concentration of displacing fluid, $M/L^3$;

$\phi$ = porosity, dimensionless;

$q(x,y)$ = injection rate of source well, $L^2/T$;

$C_i$ = source concentration, $M/L^3$;

$D$ = molecular diffusivity, $L^2/T$;

$\tau$ = tortuosity factor, dimensionless;

$\alpha_\ell$ = longitudinal dispersion coefficient, L;

$\alpha_t$ = transverse dispersion coefficient, L;

$k_x$, $k_y$ = x and y components of permeability tensor, $L^2$;

$\rho$ = density, $M/L^3$;

$g$ = accelleration due to gravity, $L/T^2$;

$\mu$ = viscosity, M/LT;

$p$ = pressure, $M/LT^2$;

$z$ = elevation above reference plane, L.

Since $\frac{\partial}{\partial x}(u_x C) = C\frac{\partial u_x}{\partial x} + u_x\frac{\partial C}{\partial x}$, equations (II.A.3) and (II.A.1) may be combined giving

$$\frac{\partial}{\partial x}(D_x\frac{\partial C}{\partial x}) + \frac{\partial}{\partial y}(D_y\frac{\partial C}{\partial y}) - u_x\frac{\partial C}{\partial x} - u_y\frac{\partial C}{\partial x} = \Phi\frac{\partial C}{\partial t} + q(C_i - C) \quad \text{(II.A.5)}$$

As pointed out in Settari, Price, and Dupont (34), equations (II.A.2) are a simplification of the general dispersion tensor neglecting the terms with cross-product derivatives. According to the above authors, this simplification is valid whenever dispersion is small and $\alpha_\ell \cong \alpha_t$.

In this work the dispersion coefficient is assumed to be constant. Hence, the final simplified equation is written as

$$D(\frac{\partial^2 C}{\partial x^2} + \frac{\partial^2 C}{\partial y^2}) - u_x\frac{\partial C}{\partial x} - u_y\frac{\partial C}{\partial y} = \Phi\frac{\partial C}{\partial t} + q(C_i - C) \quad \text{(II.A.6)}$$

The one-dimensional equation is given by

$$\frac{\partial}{\partial x}(D\frac{\partial C}{\partial x}) - u\frac{\partial C}{\partial x} = \Phi\frac{\partial C}{\partial t}, \quad 0 < x \leq \ell, \quad t > 0 \quad \text{(II.A.7)}$$

with typical boundary and initial conditions given by

$$\begin{aligned} &C(0,t) = 1 ; \quad t > 0 \\ &\frac{\partial C}{\partial x}(\ell,t) = 0 ; \quad t > 0 \\ &C(x,0) = 0 ; \quad 0 < x \leq \ell \end{aligned} \quad \text{(II.A.8)}$$

When the velocity, u, and the dispersion, D, are constant, equation (II.A.7) may be transformed into dimensionless form with $\lambda = u\ell/D$, $\xi = x/\ell$, and $\tau = Dt/\Phi\ell^2$, giving

$$\frac{\partial^2 c}{\partial \xi^2} - \lambda\frac{\partial c}{\partial \xi} = \frac{\partial c}{\partial \tau} ; \quad 0 < \xi \leq 1, \quad \tau > 0 \quad \text{(II.A.9)}$$

with boundary and initial conditions given by

$$\begin{aligned} &c(0,\tau) = 1 ; \quad \tau > 0 \\ &\frac{\partial c}{\partial x}(1,\tau) = 0 ; \quad \tau > 0 \\ &c(x,0) = 0 ; \quad 0 < x \leq 1 \end{aligned} \quad \text{(II.A.10)}$$

where $c(\xi,\tau) = C(x,t)$. The variable $\lambda$ is called the Peclet number.

## II.B Analytical Solutions

Two analytical solutions for the one-dimensional convection-diffusion equation are available in the literature. The solution most commonly used for comparisons with results of numerical solutions is given in Price, Cavendish, and Varga (28) by

$$c(\xi,\tau) = \tfrac{1}{2}\,\mathrm{erfc}\left(\frac{\xi - \lambda\tau}{2\sqrt{\tau}}\right) + \tfrac{1}{2}\exp(\lambda\xi)\,\mathrm{erfc}\left(\frac{\xi + \lambda\tau}{2\sqrt{\tau}}\right) \qquad \text{(II.B.1)}$$

This solution is derived by assuming that the right-hand boundary is an infinite distance away, and hence is not an exact solution for equations (II.A.8) and (II.A.9). However, the above authors claim that for values of $ut/\Phi\ell$ less than 2/3, equation (II.B.1) is essentially exact and may be used for comparisons with numerical solutions. Comparison with the analytical solution given below shows that this is true, provided that $\lambda$ is sufficiently large.

A second anayytical solution found in Cleary and Adrian (9) is given by

$$c(\xi,\tau) = 1 - 2\sum_{m=1}^{\infty} \exp(\lambda\xi/2 - \tau(\lambda^2/4 + \beta_m^2)) \cdot \left(\frac{\beta_m^2 \sin\beta_m\xi}{\beta_m^2 + \lambda^2/4 + \lambda/2}\right) \qquad \text{(II.B.2)}$$

where the $\beta_m$'s are positive roots of

$$\beta_m \cot\beta_m = -\lambda/2\,, \quad \beta_i > \beta_j \text{ for } i > j \qquad \text{(II.B.3)}$$

This solution is derived for boundary conditions identical to those given in equations (II.A.9) in which the right-hand boundary is a finite distance away. Unfortunately, the solution is difficult to evaluate for large $\lambda$. However, for $\lambda = 50$, the maximum difference between the solutions given by equations (II.B.1) and (II.B.2) is less than .02 (M.J.

Ungs, personal communication, July, 1976). In figures (II.B.1) and (II.B.2), the two solutions are compared for $\lambda = 5$ and for $\lambda = 50$ to numerical results from the central difference approximation described in Chapter III. The large deviation in the solutions for small $\lambda$ shows that the numerical solutions for small $\lambda$ compare better with equation (II.B.2).

The equations given in this chapter are complicated to derive and difficult to solve numerically. For certain geometries analytical solutions of the convection-diffusion equations exist for higher dimensions. However, such analytical solutions are in general not appropriate for groundwater quality models; and hence, there are no analytical solutions to compare with results from a numerical model. The technique usually employed in the literature is to test a particular method against the one-dimensional solution. If it compares favorably, the method is extended to higher dimensions. In the following chapters five numerical methods are compared against the analytical solutions of the one-dimensional convection-diffusion equation, and one of these methods, the finite element method using chapeau functions, is extended to two dimensions.

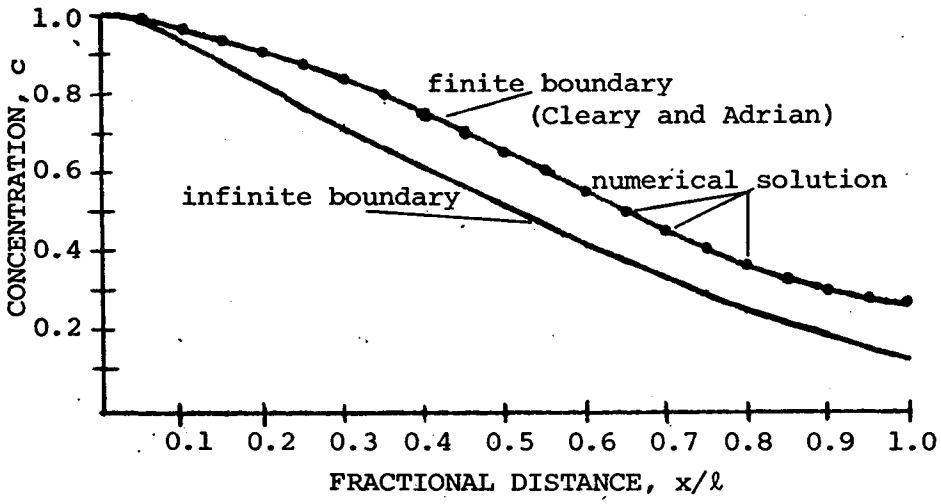


Figure II.B.1. Comparison of the two analytical solutions with the CDA method for $\lambda = 5$.

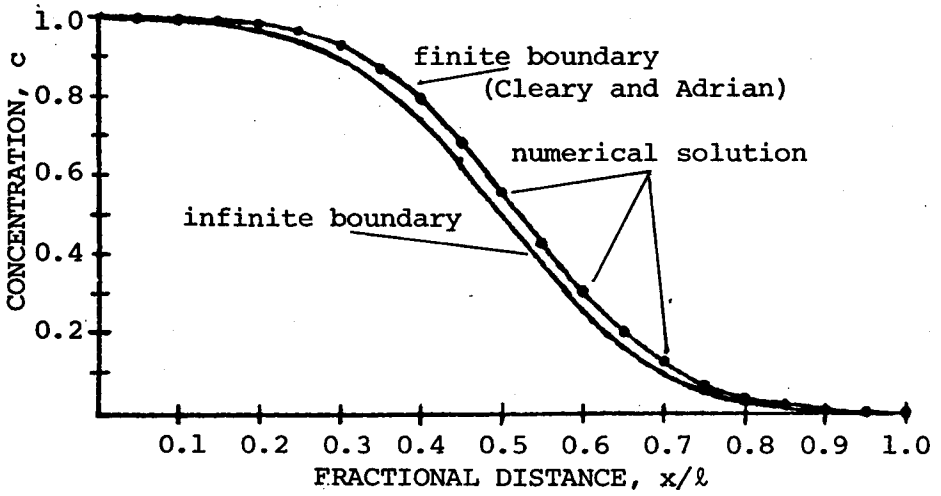


Figure II.B.2. Comparison of the two analytical solutions with the CDA method for $\lambda = 40$.

# CHAPTER III

## NUMERICAL METHODS FOR SOLVING THE ONE-DIMENSIONAL CONVECTION-DIFFUSION EQUATION

A number of methods for solving the convection-diffusion equations have been proposed. Most of the methods employ one of two techniques for discretizing the space and time variables in the differential equation: finite difference, or finite element. The term finite difference refers to discretizations formulated by replacing the derivatives in the differential equation by algebraic expressions derived from sums of truncated (finite) Taylor series expansions. A system of linear equations results which is then solved for the dependent variable. Finite element (Galerkin, variational) techniques are derived from assuming that the solution of the differential equation may be expressed as a linear combination of linearly independent functions called basis functions. The basis functions are chosen to satisfy prescribed restrictions on the continuity of high-order derivatives. The approximate solution is then substituted into an integrated form of the differential equation, and the resulting system of linear equations may be solved for the coefficients of the linear combination of basis functions. Both finite difference and finite element methods have been used extensively, and a continuing controversy exists concerning the advantages and disadvantages of each method.

All of the methods developed thus far exhibit the same types of errors: numerical dispersion and/or oscillations about the correct solution. Numerical dispersion is the term applied to results which

tend to smear the sharp concentration profile given by the analytical solution. Oscillations about unity or about zero which occur in a numerical solution are referred to as overshoot or undershoot. Some of the numerical methods have been designed to minimize oscillations at the expense of greater numerical dispersion. In a recent paper by Gray and Pinder (13), evidence is given that there is a trade-off concerning these two types of errors. More discussion of their results will be given in Chapter IV.

In this work five numerical methods are examined and compared, two finite difference and three finite element. The purpose for the comparison is to determine bounds on the space and time step sizes which keep the oscillations below a specified tolerance. In all five methods the Crank-Nicholson time discretization is employed. Hence, the methods differ in the space discretization only. In the first section of this chapter the five methods are briefly described. A more detailed description including derivation of the system of ordinary differential equations resulting from the spatial discretization, is given for each method in Appendix A. A brief review of some of the other methods which have appeared in the literature is given in the second section of this chapter.

## III.A. Methods to be Compared in this Work

All of the methods listed below are derived for a uniform mesh of length $h = \frac{1}{n}$, where n is the number of grid points over the interval [0,1]. The spatial discretization results in a system of ordinary differential equations which can be represented by the following matrix equation:

$$B \frac{d\check{c}}{d\tau} = -A\check{c} + S \qquad \text{(III.A.1)}$$

where $\check{c}(\tau) = (c(h,\tau), c(2h,\tau),..., C(1,\tau))$. The central difference time discretization approximates the time derivative at time $\tau + \Delta\tau/2$ by

$$\frac{d\check{c}}{d\tau}(\tau + \tau/2) = \frac{\check{c}(\tau + \Delta\tau) - \check{c}(\tau)}{\Delta\tau} \qquad \text{(III.A.2)}$$

Using the Crank-Nicholson approximation, the matrix equation is given by

$$B \frac{\check{c}(\tau + \Delta\tau) - \check{c}(\tau)}{\Delta\tau} = -A\check{c}(\tau + \Delta\tau/2) + S \qquad \text{(III.A.3)}$$

where $\check{c}(\tau + \Delta\tau/2) = \frac{\check{c}(\tau) + \check{c}(\tau + \Delta\tau)}{2}$

The system is then solved implicitly for $\check{c}(\tau + \Delta\tau)$. The five methods to be compared are the following:

1. Central Difference Approximation (CDA). The CDA method used the standard, second order correct, central difference approximation for the spacial derivatives.

2. Non-Central Difference Approximation (NCDA). The NCDA method used the standard second order correct difference approximation for the second derivative in the diffusion term and a second order correct three point backward difference approximation for the first derivative in the convective term.

3. Finite Element with Chapeau Basis Functions. The chapeau basis functions are piecewise-linear polynomials. The system of ordinary differential equations resulting from this formulation is very similar to that of the CDA method. Price, Varga, and Warren (29) approximate the right-hand boundary conditon by using piecewise-quadratic basis

functions over the last interval. If chapeau basis functions are used throughout, a slightly different linear system results, but the numerical solutions are virtually identical.

4. Finite Element with Cubic Hermite Basis Functions. The cubic Hermite basis functions used in this work are the piecewise-cubic polynomials with continuous first derivatives defined in Price, Varga, and Warren (29). Two linear equations are required for each node point, but half as many node points are required for the same or better accuracy than lower order methods.

5. Lumped Matrix Approximation. Unlike finite difference methods, in finite element approximations the matrix multiplying the time derivative is not the identity matrix. To avoid inverting this matrix, the matrix is "lumped," i.e., the matrix multiplying the time derivative is replaced by the identity matrix. Otherwise, the derivation is the same as for finite element methods. In this work, the lumped matrix approximation is applied to the finite element method with chapeau basis functions.

## III.B. Other Methods for Solving the Convection-Diffusion Equations

Both the finite element and the finite difference techniques offer a wide variety of solution methods. The five methods chosen for comparison in this work are very basic applications of finite element and finite difference techniques. This section includes a brief discussion of how the basic techniques can be extended to develop new methods of solution.

An intriguing exposure to the possibilities for developing new finite element solution methods is given by Rachford (30). Options

open to the finite element programmer include choice of the degree of the polynomial basis functions, and, for piecewise polynomials, the number of continuous derivatives, variable grids, and collocation. Collocation is a method in which the solution is forced to satisfy the differential equation at Gauss points, the points required for Gaussian quadrature integration of the integrals which result from the finite element procedure (see Appendix B.3). Price, Cavendish, and Varga (28) have developed a method called variable interpolation in which high-order basis functions are used where the function values are highly variable and low-order basis functions are used elsewhere. Smith (36) uses finite element integration for the time discretization as well as the space discretization. Other models using the finite element techniques are given in the list of references (14, 15, 16, 22, 34, 43).

Finite difference formulas for derivatives are easily generated by summing truncated Taylor series expansions. Examples of this are given in Appendix A. Clever use of this technique allows the generation of higher order formulas; however, more points are usually required for the evaluation of each derivative. Finite difference solutions require inversion of a banded matrix. The more points required to evaluate the derivatives, the wider the band; hence, more computations are required. A decision which both finite element and finite difference programmers must make is whether to use low order formulas on a fine grid or high order formulas on a coarse grid. Usually this decision is based on the geometry of the problem.

Stone and Brian (39) offer a flexible finite difference technique based upon weighted differences. Their difference equation is the following:

$$\frac{-D}{(\Delta x)^2}\left[\tfrac{1}{2}(c_{i-1,n+1} - 2c_{i,n+1} + c_{i+1,n+1}) + \tfrac{1}{2}(c_{i-1,n} - 2c_{i,n} + c_{i+1,n})\right] + \frac{u}{\Delta x}\left[a_1(c_{i+1,n} - c_{i,n}) + a_2(c_{i,n} - c_{i-1,n}) + a_3(c_{i+1,n+1} - c_{i,n+1}) + a_4(c_{i,n+1} - c_{i-1,n+1})\right] + \frac{1}{\Delta\tau}\left[b_1(c_{i,n+1} - c_{i,n}) + b_2(c_{i-1,n+1} - c_{i-1,n}) + b_3(c_{i+1,n+1} - c_{i+1,n})\right] = 0 \qquad \text{(III.B.1)}$$

where $c_{i,j} = c(i\Delta x, j\Delta t)$. The weighting coefficients $a_1$, $a_2$, $a_3$, $a_4$, $b_1$, $b_2$, and $b_3$ are arbitrary constants which satisfy $a_1 + a_2 + a_3 + a_4 = 1$ and $b_1 + b_2 + b_3 = 1$. The Crank-Nicholson approximation used for the second derivative is also a weighted finite difference approximation with equal weight given to values for each time step. Stone and Brian ( 39 ) suggest solving three or more equations with different weighting coefficients in a cyclical manner through time. A good summary of numerical solutions for the convection-diffusion equation, including an extension of the Stone and Brian scheme to two and three dimensions using an alternating direction solution technique, is found in Shamir and Harleman ( 35 ).

An interesting fact is that the set of weighting coefficients recommended by Stone and Brian for a one equation solution are exactly those that can be derived with finite element techniques using chapeau basis functions. Advocates for the use of finite difference techniques claim that such methods as the use of weighted differences make possible equally good, or better, models than can be developed through finite element techniques. A recent paper by Laumbach ( 20 ) improves upon the formulation of Stone and Brian to develop a high-accuracy finite

difference technique which appears to be superior to the finite element model using chapeau basis functions. Other finite difference models examined in the literature are included in the list of references (21).

An adaptation of the finite difference method which has received some attention in the literature is given by Peaceman and Rachford (24). They first examine the effect of using a first-order correct backward difference formula for the first derivative in the convection term instead of the central difference used in the CDA method. This process, called upstream weighting, eliminates oscillations in the solution, but it causes unacceptable numerical dispersion. Returning to use of the CDA method, the authors suggest a scheme in which the concentraion at each node i, $c_i$ is compared to the concentration at the next node, $c_{i+1}$, after each time step. If $c_{i+1}$ exceeds $c_i$, then the excess is added to $c_{i+2}$ and subtracted from $c_i$. This process is called transfer of overshoot.

The remaining method which must be included in any discussion of solutions of the convection-diffusion equation is the method of characteristics (MOC). This method, first developed by Gardner, Peaceman, and Pozzi, recognizes that for large values of the Peclet number, $\lambda$, the equation behaves more like a hyperbolic than a parabolic differential equation, and, hence, a method using characteristics is appropriate. MOC models require a large number of grid points and are inaccurate for small values of the Peclet number. In groundwater quality and reservoir engineering problems the Peclet number is large enough that the MOC method is appropriate. Bredehoeft and Pinder used the MOC solution technique for their model of the groundwater contamination at Brunswick, Georgia.

# CHAPTER IV

## COMPARISON OF FIVE NUMERICAL METHODS FOR SOLVING THE ONE-DIMENSIONAL CONVECTION-DIFFUSION EQUATION

As with most engineering problems, there are many trade-offs associated with numerical solutions of the convection-diffusion equations. Models which are simple to derive may require prohibitive amounts of computer space and processor time. A more complicated technique may require less computer time and space, but it may be difficult to extend to higher dimensions, and boundary conditions may be more difficult to incorporate. Certain discretizations may eliminate oscillations, but they suffer from severe numerical dispersion errors. A good comparison of the solution methods must take these trade-offs into account. No method has been found to be completely satisfactory. Hence, it is useful to develop certain criteria for determining whether a particular method produces adequate results. For the one-dimensional convection-diffusion equation, the important parameter is the Peclet number, $\lambda$. Most of the methods work well for small values of $\lambda$, but for large values of $\lambda$ numerical dispersion and oscillations appear in the numerical solutions (results for the models in this work indicate that significant errors occur for $\lambda > 5n$). The objective behind the comparisons to be given in this work is to find the minimum number of required nodes, n, and the maximum allowable time step, $\Delta\tau$, given $\lambda$ and the accuracy required of the solution.

In the first section the theoretically derived limits on the spacing, $h = \Delta\xi$, and the time step, $\Delta\tau$, for numerical solutions of equation

(II.A.8) are examined. In the second section results of numerical experiments show how these limits may be adjusted if small oscillations in the solution are tolerated.

## IV.A. Theoretical Derivation of Discretization Bounds

Some important results concerning oscillations in the solution are given in Price, Varga, and Warren (29). All of the methods considered by these authors used non-weighted finite differences. Hence, the matrix differential equation derived from the space discretization is written in the form

$$\frac{d\tilde{c}}{d\tau} = -A\tilde{c} + S \qquad \text{(IV.A.1)}$$

Their analysis is based on properties of the matrix A related to the eigenvalues of A. If the matrix A has distinct positive real eigenvalues, then the equation for the solution of equation (IV.A.1) reveals that the solution is non-oscillatory. The authors give theoretical proofs that the solution to the semi-discrete CDA equations is non-oscillatory for $h \leq 2/\lambda$. Since $h = \frac{1}{n}$, where n is the number of grid points, the above criterion can be written in terms of $\lambda$ and n as

$$n \leq \lambda/2 \qquad \text{(IV.A.2)}$$

They also show that the NCDA method is non-oscillatory for all values of h. These results are derived from proofs that for a given value of $\lambda$, the matrix A for the CDA method has distinct positive real eigenvalues for $0 \leq \alpha \leq 1$ where $\alpha = \lambda h/2$, and for the NCDA method the matrix A has distinct positive real eigenvalues for all values of $h > 0$. The other

important result in this article is that oscillations due to the time discretization are eliminated for the Crank-Nicholson scheme whenever

$$\Delta\tau \leq 2/\max \mu_i, \quad 1 \leq i \leq n \tag{IV.A.3}$$

where each $\mu_i$ is an eigenvalue of the matrix A. The authors state that their numerical experiments indicate that oscillations are eliminated for all practical purposes if

$$\Delta\tau \leq 1/\min \mu_i, \quad 1 \leq i \leq n \tag{IV.A.4}$$

Equations (IV.A.2) and (IV.A.3) give restrictions on $\Delta\tau$ and n for preventing oscillations in the solution. However, it is clear that for large values of $\lambda$ the number of nodes required for the CDA method becomes prohibitive. Unfortunately, typical parameters for groundwater quality models produce values of $\lambda$ exceeding $10^4$. Equation (IV.A.3) is valid only when the eigenvalues of A are real. Thus, for the CDA method, this criterion works only when $h \leq 2/\lambda$. Furthermore, a criterion based on the eigenvalues of a matrix is difficult to apply, since the eigenvalues must first be computed. For the CDA method, equation (IV.A.3) can be simplified considerably by considering the eigenvalues of A when $h = 2/\lambda$. Examination of equation (B7) in Appendix B reveals that in this case, A is a lower triangular matrix with each diagonal element given by $2/h^2$. Thus, equation (IV.A.3) becomes

$$\Delta\tau \leq h^2 \quad \text{or} \quad \Delta\tau \leq 4/\lambda^2 \tag{IV.A.5}$$

when $h = 2/\lambda$. Since more nodes will not decrease the maximum $\Delta\tau$ allowed, the criterion is given by

$$\Delta\tau_{max} = 4/\lambda^2 \quad \text{for} \quad h \leq 2/\lambda \tag{IV.A.6}$$

The above criteria apply to errors due to oscillations in the solution. Lantz (19) examines the truncation error in the finite difference approximations to the convection-diffusion equation to derive expressions for the magnitude of the numerical dispersion. His procedure is to express the finite difference formulas as Taylor series expansions, substitute the Taylor series into the differential equation in place of the corresponding partial derivatives, and collect like derivative terms. This results in some extra terms involving the second partial derivative when first order approximations are used for the first partial derivatives in the differential equation. These additional terms determine what Lantz calls numerical diffusivity. In certain cases, appropriate choice of h and $\Delta\tau$ will reduce the numerical diffusivity to zero. The Crank-Nicholson time discretization and the CDA space discretization both are second order correct and hence do not provide terms for the numerical diffusivity. Upstream weighting, which implies that a backward difference formula is used to approximation the first partial derivative, results in numerical diffusivity equal to h/2 when the Crank-Nicholson time discretization is used. Since the methods to be compared in this work are all at least second order correct, this method of predicting errors in the solution cannot be used. However, this approach is exactly what Laumbach (20) used to determine a weighting factor for the time discretization that leads to a finite difference equation which is fourth order correct in space and time for larger values of $\lambda$ when $h \geq \lambda\Delta\tau$. Laumbach includes third order terms in his

Taylor series expansion and makes use of the fact that when $\lambda >> 1$, $\frac{2C}{2\tau} \cong -\lambda\frac{2C}{2\xi}$.

In a recent paper by Gray and Pinder (13), Fourier series analyses are used to understand better the causes of numerical dispersion and oscillations in the numerical solutions. Similar analysis has been used before by Shamir and Harleman (35) and Stone and Brian (39), but in the work by Gray and Pinder the comparisons of different numerical methods which can be made are clearly indicated. In particular, different weighted time discretizations are compared for finite difference and finite element methods. Their procedure is to substitute the Fourier series components into the fully discretized equation, solve the resulting equation for the eigenvalues of the Fourier series representation of the numerical solution, and from the eigenvalues compute amplitude modifications and phase lags in the Fourier harmonics for the particular numerical method being tested. The results show that both finite element and finite difference solutions show greater phase lags and amplitude modifications in the shorter wavelengths. The fully implicit time discretization produces greater phase lag and more damping in the shorter wavelengths than the semi-implicit Crank-Nicholson time discretization for both finite element and finite difference. Hence, there appears to be a trade-off: methods which propagate the shorter wavelengths more accurately seem to modify their amplitude more, while accurate amplitude production sacrifices correct phase propagation. When the shorter wavelengths are unimportant to the correct analytical solution, as they are for small values of the Peclet number, if these wavelengths are damped as in the finite element method, the errors will

be small. But if, as in the CDA method, the shorter wavelengths are amplified, then the phase lag produces both oscillations and numerical dispersion. Their conclusions included the following: that finite difference methods were consistently inferior to finite element, that dispersion correction factors suggested by Chaudhari (7) are more effective in improving the accuracy of finite element schemes than finite difference, that upstream weighting causes excessive damping over a wide range of wavelengths, and that minimizing oscillations about unity by appropriate weighting in the time discretization increases the numerical dispersion in the solution.

## IV.B. Discretization Bounds Based on Numerical Experiments

Price, Varga, and Warren (29) show that for $\Delta\tau$ sufficiently small, oscillations in the solution using the CDA or the NCDA method are due to the space discretization alone. Hence, reducing $\Delta\tau$ further will not reduce the oscillations in the solution. Since these authors show that oscillations appear when the matrix A has complex eigenvalues, and since the expression for the maximum $\Delta\tau$ is a function of the maximum eigenvalue of A, a seemingly reasonable approach is to examine the eigenvalues of A for the five methods. For $n = 20$ ($h = .05$), the behavior of the maximum real and imaginary parts of eigenvalues of the matrix A for the CDA, chapeau and cubic Hermite methods is shown in Figure IV.B.1. Several interesting features are apparent in this diagram. First, all three methods show a change in the eigenvalues at or near a Peclet number of 40; that is when $n = \lambda/2$. For $\lambda$ slightly greater than 40, complex eigenvalues begin to appear, signalling the beginning of oscillatory behavior in the solution. If results similar to equation

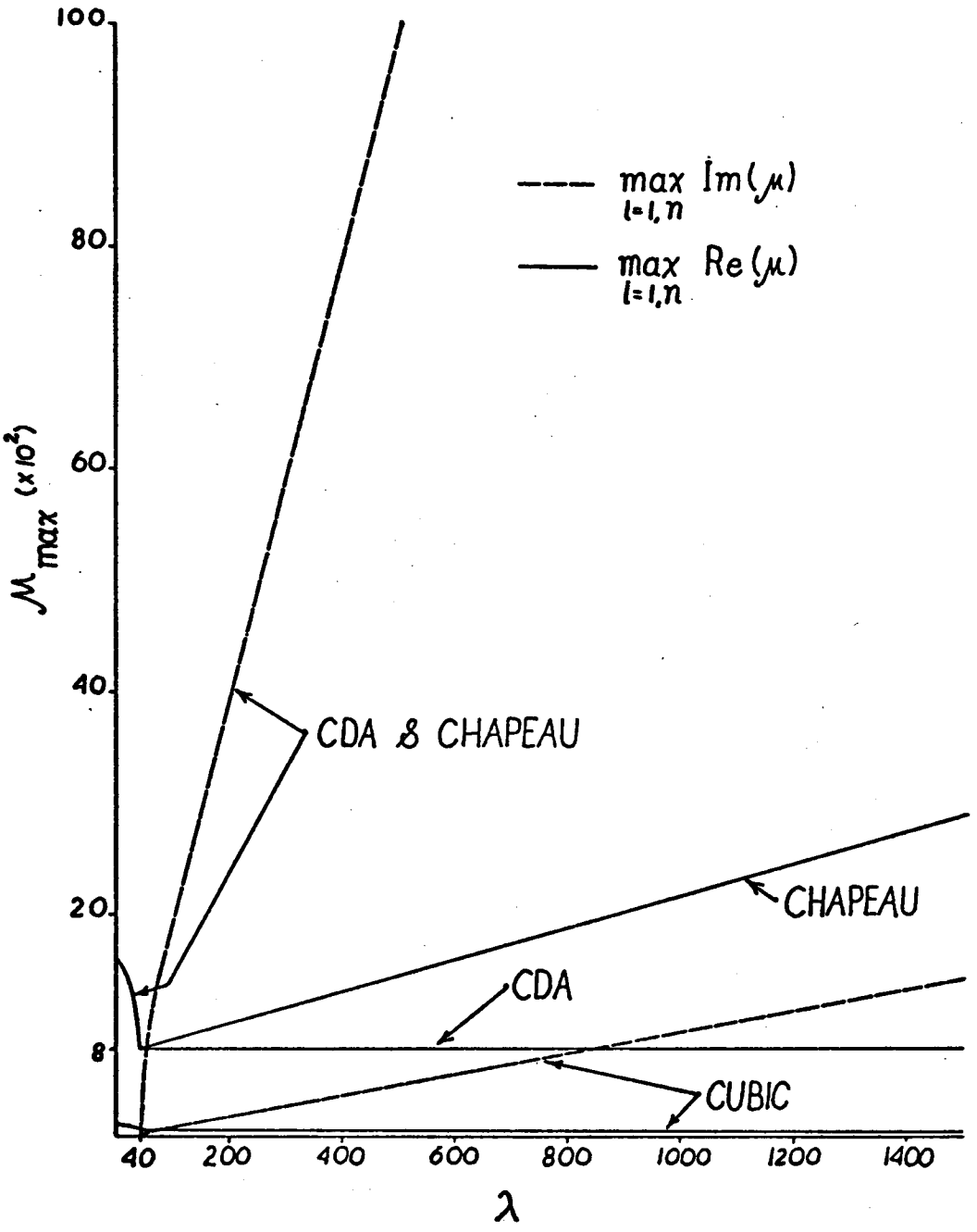


Figure IV.B.1. Maximum real and imaginary parts for eigenvalues of Matrix A for three of the numerical methods.

(IV.A.3) can be derived for finite element solutions, then the diagram suggests that the cubic Hermite solution method should be accurate for much larger time steps. Furthermore, if the magnitude of the imaginary parts of the eigenvalues is important, the cubic Hermites might be expected to allow larger space steps as well. The similarity between the CDA and chapeau methods is suggested by the nearly identical behavior in the eigenvalues for the two methods, the only appreciable difference being in the maximum real part of the eigenvalues for $\lambda > 40$. For the CDA method the real parts of the eigenvalues for $\lambda > 40$ are identically equal to $800 = 2n^2$. Additional calculations made for $n = 10$ indicate that these results are reproducible for other values of n. One last result is that the magnitude of the maximum eigenvalue for the CDA and chapeau method is approximately $\lambda \cdot n$. This suggests that the maximum $\Delta\tau$ sufficiently small to avoid oscillations due to the time discretization might be given by $2/\max \mid \mu_i \mid = 2/\lambda n$, $1 \leq i \leq n$. However, numerical results indicate that the oscillations in the solution are reduced if a smaller $\Delta\tau$ is used. The maximum $\Delta\tau$ for $n < \lambda/2$ suggested by a number of numerical experiments is given by

$$\Delta\tau_{max} = 1/10\lambda n \quad \text{or} \quad \Delta\tau_{max} = \frac{\Delta x}{10u} \tag{IV.B.1}$$

Varying $\Delta\tau$ around this bound results in the following behavior: $\Delta\tau = 2\Delta\tau_{max}$ causes oscillations in the solution for $\lambda = 2n$; and, $\Delta\tau = \Delta\tau_{max}/10$ does not produce results which are significantly different from results for $\Delta\tau = \Delta\tau_{max}$. Hence, $\Delta\tau \leq \frac{1}{10\lambda n}$ is sufficiently small to avoid errors due to the time discretization. This bound on $\Delta\tau$ appears to work for the CDA and all three finite element methods.

The behavior of the eigenvalues shown in Figure IV.B.1 indicates that oscillations in a numerical solution using any one of the three methods included there are prevented for $n \geq \lambda/2$ as given in equation (IV.A.2). Numerical experiments for values of $\lambda$ ranging from 40 to 320 support this conclusion. For large values of $\lambda$, the number of nodes required is prohibitive. However, numerical experiments reveal that if small oscillations (less than 0.1) are acceptable, the number of nodes required can be considerably reduced for the finite element methods.

Using the criterion for $\Delta\tau$ given by equation (IV.B.1), the minimum number of nodes, $n_{min}$, required for a given value of $\lambda$ to prevent oscillations exceeding a specified value was found through the following procedure: for a particular number of nodes, n, different values of $\lambda$ were tried until the requirement that all of the computed values throughout the time interval $0 \leq \tau \leq 1/\lambda$ were less than the specified tolerance. The minimum $\lambda$ for which this is true satisfies the relation that the given n is $n_{min}$ for that $\lambda$. In each trial, the time step was that given by equation (IV.B.1) with the appropriate values for $\lambda$ and n.

This procedure was applied to the CDA method and the first two finite element methods. Figure IV.B.2 shows the results of the numerical experiments for specified tolerances of 1.1 and 1.01. Over the range of the values tested, the dependence of $n_{min}$ on $\lambda$ appears to be linear. Examination of the figure reveals that for a given $\lambda$, as expected, the cubic Hermites require the least nodes to achieve a specified accuracy. Since $\Delta\tau$ is inversely proportional to n, the cubic functions allow larger time steps to be used without penalty, thus requiring fewer computations, and hence, less processor time. The results diagrammed in Figure IV.B.2 are summarized in the following table:

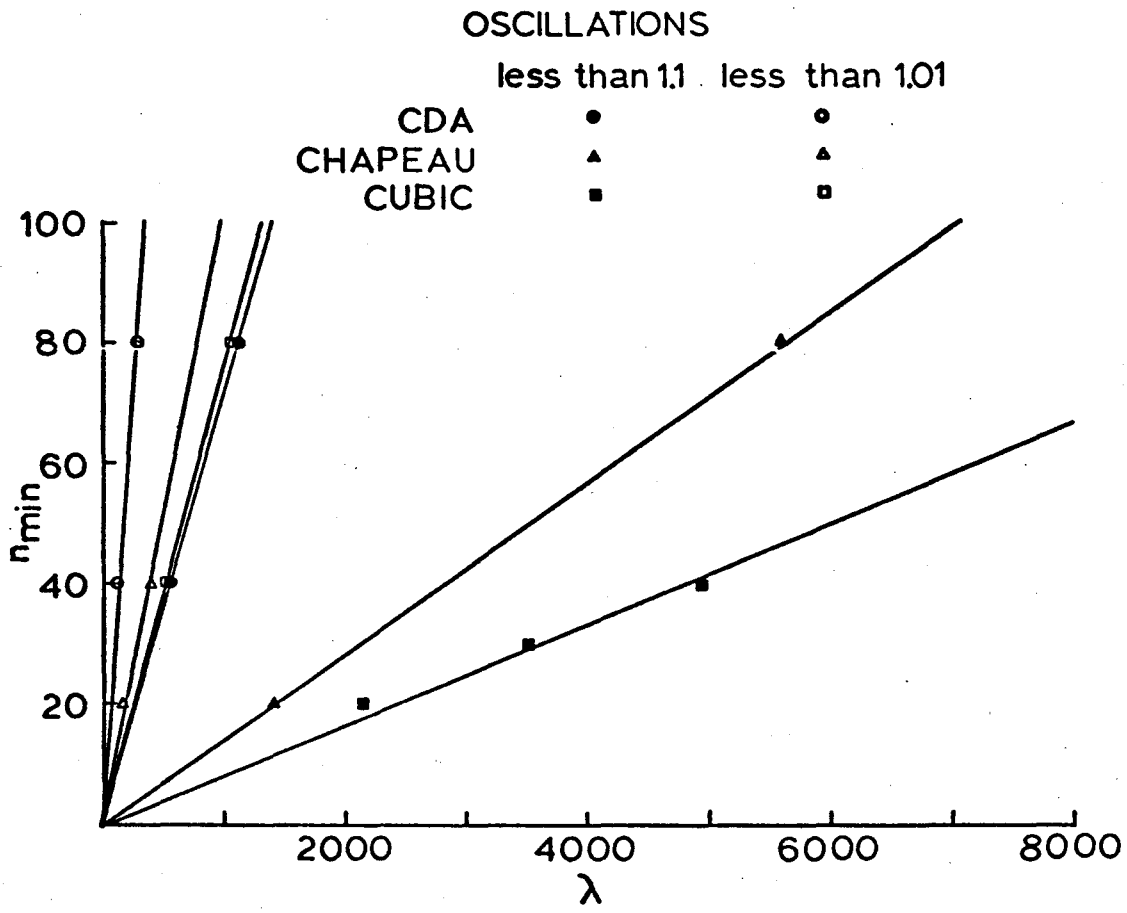


Figure IV.B.2. Minimum number of nodes required for a given λ and specified tolerance.

OSCILLATIONS

| | Less than 1.01 | Less than 1.1 |
|---|---|---|
| CDA | $n \geq \lambda/3.5$ | $n \geq \lambda/13$ |
| CHAPEAU | $n \geq \lambda/10$ | $n \geq \lambda/70$ |
| CUBIC | $n \geq \lambda/13$ | $n \geq \lambda/120$ |

TABLE IV.B.1

Some examples which help to illustrate how oscillations may be caused by either the space or the time discretization are given in Figures IV.B.3 through IV.B.7. The first three examples use the CDA method. Although less pronounced, the behavior of the finite element methods is the same as is illustrated in these three figures. Figure IV.B.3 shows that the numerical solution agrees with the second analytical solution (see comparison of the two analytical solutions given in Chapter II) for $n = \lambda/2$ and $\Delta\tau = \frac{1}{10\lambda n}$. In Figure IV.B.4, $\Delta\tau$ is increased by a factor of 40. These oscillations are caused by the excessive time step size. In Figure IV.B.5, $\Delta\tau$ is restored to an acceptable value, and the spacing is increased by reducing the number of nodes by a factor of four. In this case, both oscillations and numerical dispersion are evident. In Figures IV.B.6 and IV.B.7, the NCDA method is used. For $n = \lambda/2$ and $\Delta\tau = 1/10\lambda n$, the NCDA method works as well as any of the methods. Figure IV.B.6 reveals that the effect of increasing the spacing is manifested by numerical dispersion and small oscillations about zero. The oscillations about zero are barely perceptable in this example, but in a later figure oscillations about zero are quite pronounced for the NCDA method. Oscillations about unity do not appear

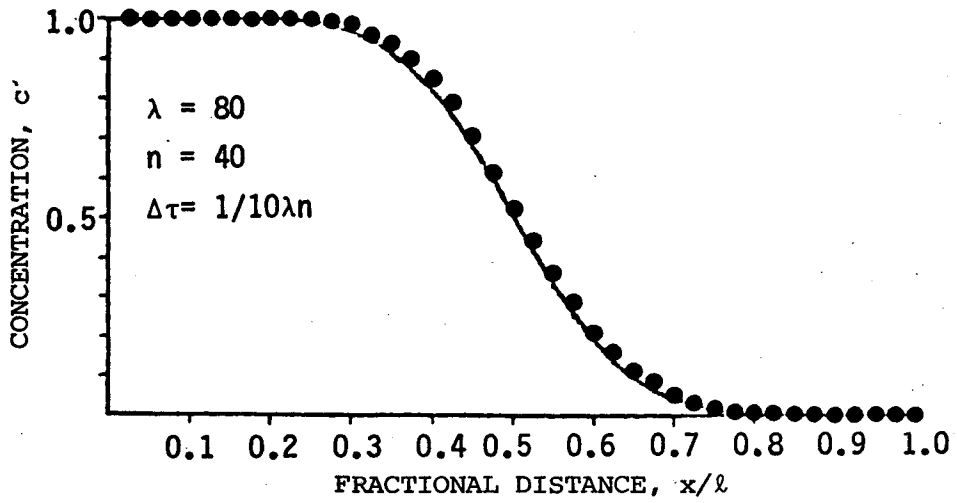


Figure IV.B.3. Results from CDA method showing no oscillations for small $\Delta\tau$ with $n \geq \lambda/2$.

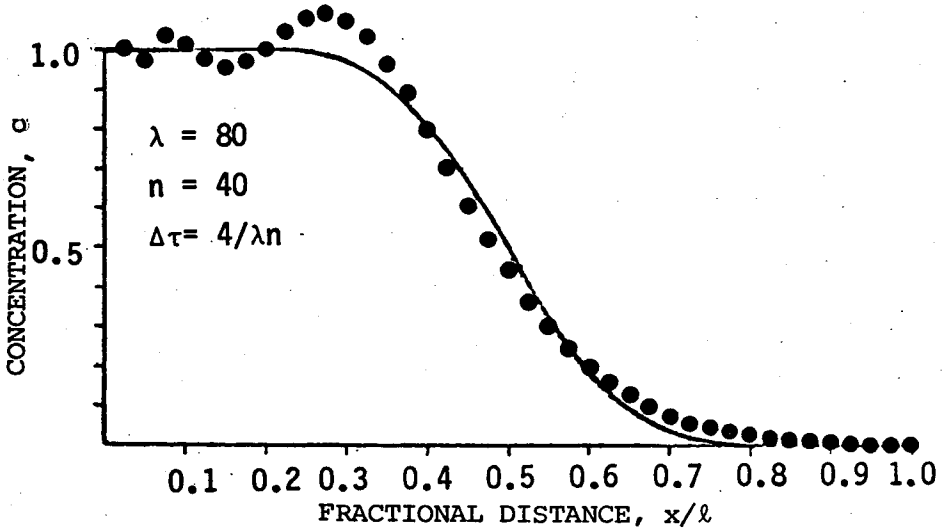


Figure IV.B.4. Results from CDA method showing oscillations caused by large $\Delta\tau$.

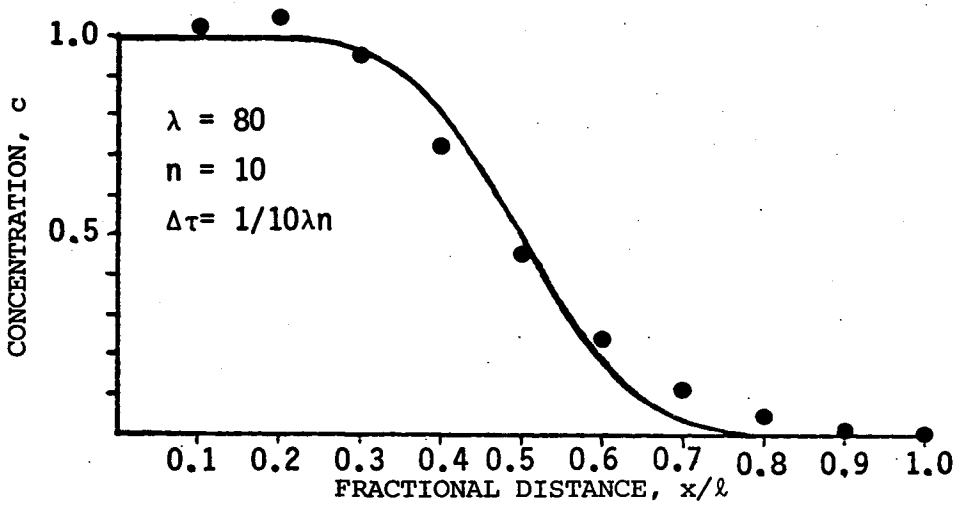


Figure IV.B.5. Results from CDA method showing oscillations and numerical dispersion caused by small n.

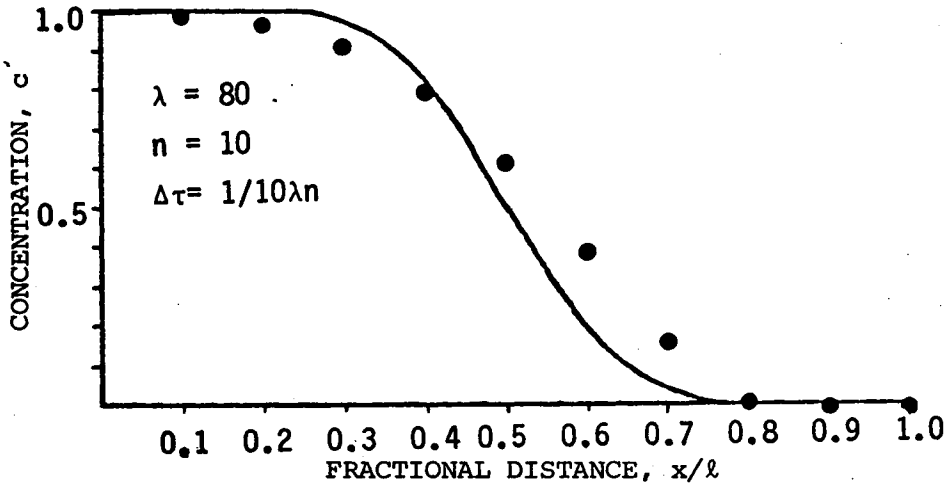


Figure IV.B.6. Results from NCDA method showing small oscillations about zero and numerical dispersion.

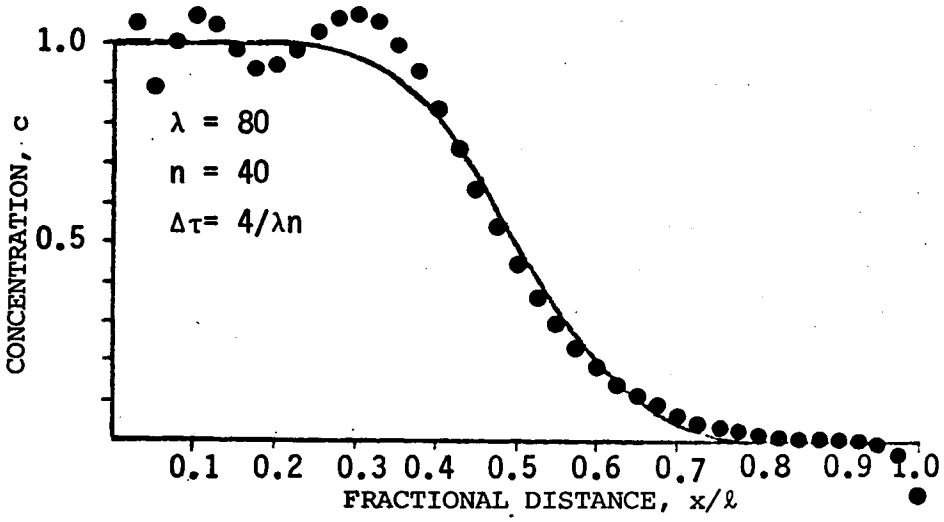


Figure IV.B.7. Results from NCDA method showing oscillations caused by large Δτ.

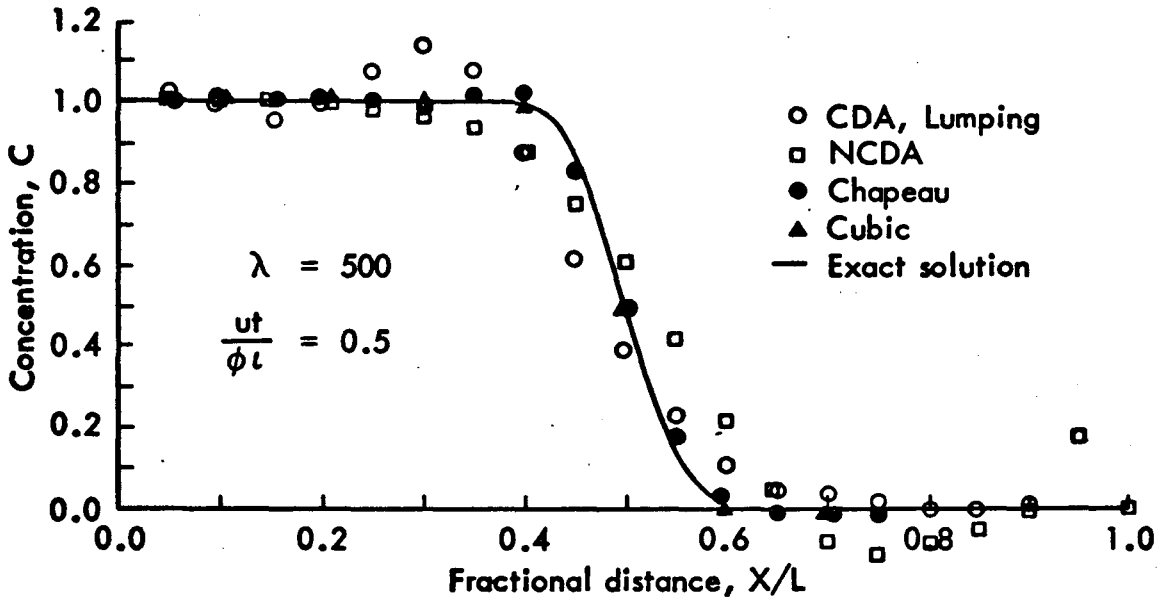


Figure IV.B.8. Comparison of the five numerical methods for n = 20.

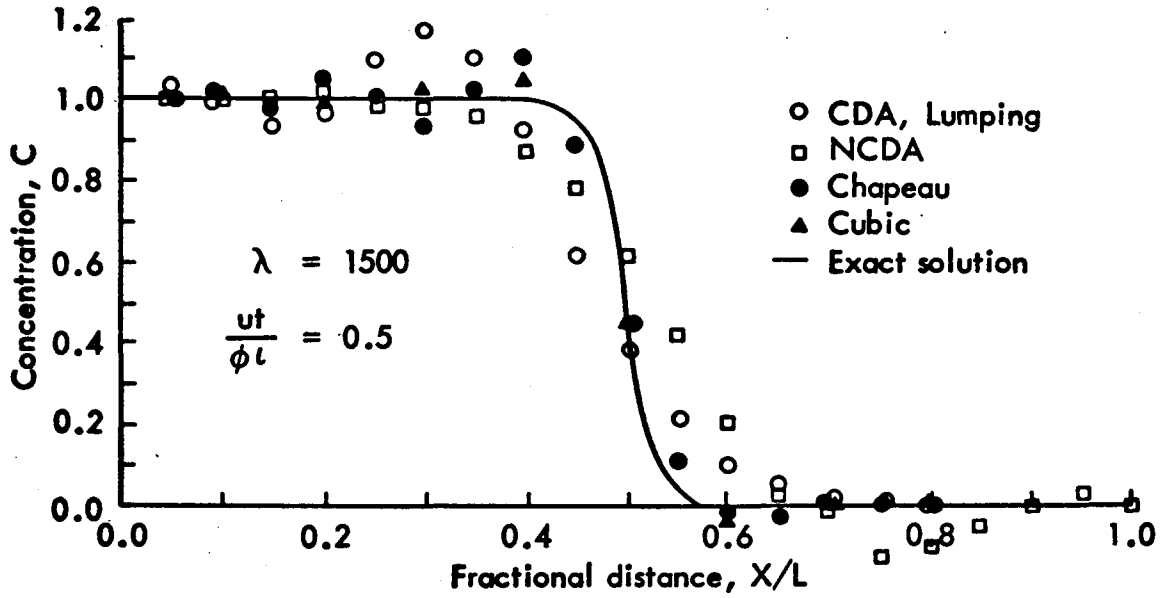


Figure IV.B.9. Comparison of the five numerical methods for n = 20.

unless $\Delta\tau$ is too large, as is shown to be the case in Figure IV.B.7.

Comparisons of all five numerical methods appear in Figures IV.B.8 and IV.B.9 for $\Delta\tau$ given by equation (IV.B.1) where n = 20 and for $\lambda$ = 500 and 1500, respectively. These values for $\lambda$ were chosen to illustrate the oscillations and numerical dispersion due to the space discretization when the bounds on the spacing given in Table IV.B.1 are exceeded. Reference to Figure IV.B.2 indicates that oscillations in the first two finite element techniques using Chapeau and cubic Hermite basis functions should be less than 10%, and Figure IV.B.8 is consistent with that result. For $\lambda$ = 1500 only the NCDA and the cubic Hermite methods have oscillations within the 10% tolerance. The NCDA method, however, exhibits considerably more numerical dispersion in both examples than any of the other methods. The CDA and Chapeau methods exhibit oscillations exceeding 1.1 for $\lambda$ = 1500. Finally, the lumped matrix method appears to give results that are nearly identical to the results of the CDA method, and hence, loses all of the accuracy advantage of the finite element approximation.

In conclusion, it is apparent that the finite element methods do reduce oscillations in the solution when compared to finite difference methods. The simple criterion in equation (IV.B.1), plus the results in Table (IV.B.1) indicate bounds for $\Delta\tau$ and $h = \frac{1}{n}$ for specified $\lambda$ and the required accuracy. It should be mentioned, however, that although oscillations about unity can be controlled through the use of an adequate number of node points, the NCDA and finite element methods show oscillations about zero in the first few time steps. For the finite element methods, these oscillations are of small magnitude. But for

the NCDA method oscillations about zero may produce concentration values less than -.1. In addition, these oscillations remain in the NCDA solution throughout most of the time of interest.

# CHAPTER V

# EXTENSION TO A TWO-DIMENSIONAL FINITE ELEMENT MODEL USING CROSS-PRODUCTS OF CHAPEAU BASIS FUNCTIONS ON A SQUARE GRID

The application of the two-dimensional convection-diffusion equation of primary interest in this work is groundwater quality modeling. Although the overall velocities and concentration fluctuations are less than for petroleum reservoir models, both applications are complicated by several factors. The flow patterns are fairly random and may require tracing the concentration profile past a producing well. Furthermore, the models may be required to predict near steady state conditions. Boundary conditions for wells producing contaminant at varying concentrations are difficult to specify because the velocities near the well vary increasingly in magnitude and direction, and the mass balance must take into account the mass removed from the system.

The two-dimensional model developed for this work is a simplified finite element model using cross-products of the chapeau basis functions on a square grid pattern. The objective of this work is to do preliminary testing on the model to determine its applicability to typical groundwater quality problems.

## V.A. Two-Dimensional Geometries to be Modeled

In order to concentrate on the effects of convection and diffusion, the groundwater flow, as shown in equation (II.A.3) is assumed to be steady state. This eliminates the necessity to compute new velocities before calculating the concentration profile for each time step. There are a number of possible geometries which produce steady state velo-

cities. Four steady state flow patterns are shown in Figures V.A.1. (a)-(d). The first flow pattern represents a constant unidirectional velocity field. This flow pattern is used with the one-dimensional convection-diffusion equation given in Chapter II. The second flow pattern represents a producing well in a constant unidirectional velocity field. The third flow pattern represents a producing well alongside an equipotential line. The last flow pattern represents the dipole field produced by two wells with equal pumping rates, one producing, the other injecting contaminant at a constant concentration.

Approximate boundary conditions for the convection-diffusion equation are shown in Figures V.A.1.(e) and (f). The impermeable boundaries are in contradiction with the velocity flow patterns unless one makes the unrealistic assumption that contaminant flow is impeded at the boundaries while groundwater flow is unaffected by the boundary. However, except for the right-hand condition, the impermeable concentration boundary is appropriate for the first flow pattern, and is a fairly valid approximation for the second flow pattern, because the flow is nearly parallel to the lateral boundaries. For the remaining two flow geometries, the impermeable concentration boundaries are a valid approximation as long as the concentration gradient remains small near the boundary.

Preliminary tests of the model developed for this work were on the first two geometries. The model also provides the other two flow geometries and the corresponding concentration boundary conditions, but these have not been sufficiently tested.

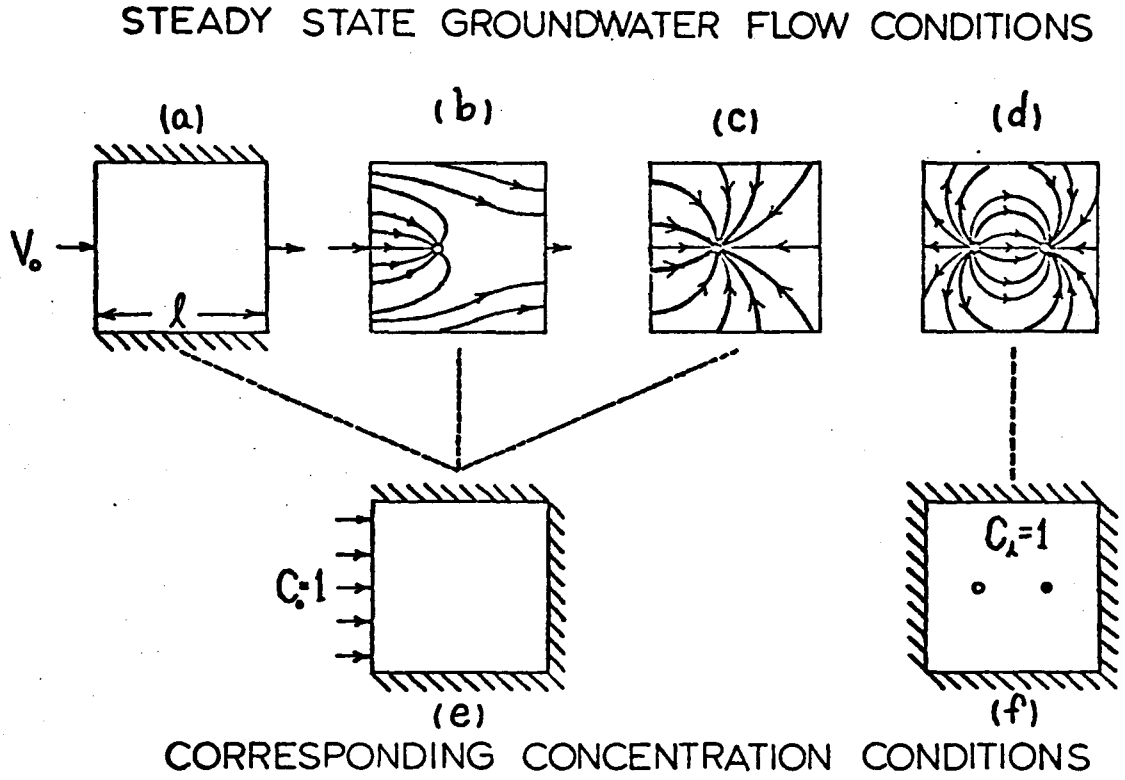


Figure V.A.1. Boundary conditions for the two-dimensional model.

V.B Description of the Two-Dimensional Model.

In this section a brief discussion of the development of the two-dimensional finite element model using chapeau basis functions is given. Details of the required mathematics are included in the appendix.

As pointed out in Chapter III, finite element models approximate the solution of the partial differential equation by a linear combination of basis functions. The basis functions used in this work are cross-products of chapeau basis functions $w(x)\cdot\tilde{w}(y)$. To incorporate the boundary conditions suggested in Figure V.A.1.(e), the $w(x)$ must satisfy the conditions that $w(0) = 0$ and $\frac{dw}{dx}(\ell) = 0$; and the $\tilde{w}(y)$ must satisfy the conditions that $\frac{d\tilde{w}}{dx}(0) = \frac{d\tilde{w}}{dx}(\ell) = 0$, where $\ell = n\Delta x$, and n is the number of nodes. For the boundary conditions in Figure V.A.1.(f), the $w(x)$ must satisfy $\frac{dw}{dx}(0) = \frac{dw}{dx}(\ell) = 0$. In addition, boundary basis products $w_\partial(x)\cdot\tilde{w}_\partial(y)$ are required for the constant concentration boundary. These are specified by the requirement that $w_\partial(0) = 1$, $\frac{dw_\partial}{dx}(\ell) = 0$, and $\tilde{w}_\partial(y) = 1$. With the basis functions thus chosen, the solution is approximated by the following:

$$C_n(x,y,t) = \sum_{i=1}^{n}\sum_{j=1}^{n} C_{n,i,j}(t)w_i(x)\tilde{w}_j(y) + w_\partial(x)\tilde{w}_\partial(y) \qquad \text{(V.B.1)}$$

This approximation must satisfy an integrated form of the differential equation given by

$$\int_F\int [\Phi\frac{\partial C_n}{\partial t} - D\left(\frac{\partial^2 C_n}{\partial x^2} + \frac{\partial^2 C_n}{\partial y^2}\right) + v_x\frac{\partial C_n}{\partial x} + v_y\frac{\partial C_n}{\partial y}]w_k(x)dx\ \tilde{w}_l(y)dy \qquad \text{(V.B.2)}$$

As shown in Appendix C, as a first approximation the velocities are assumed constant over one grid block. The velocity vectors are computed from the analytical solution at the grid points. The assumption that the velocities are constant allows their removal from the integration

over the basis functions. The remaining integrations are straightforward. In addition, the initial conditions are approximated by

$$\| C_n(x,y,0) \|_{L^2[F]} = \min_{\alpha_{i,j}} \| \sum_{i=1}^{n} \sum_{j=1}^{n} \alpha_{i,j} w_i \tilde{w}_j + w_\partial \tilde{w}_\partial \|_{L^2[F]} \qquad \text{(V.B.3)}$$

These equations determine a set of ordinary differential equations of the form

$$B \frac{d\tilde{C}_n}{dt} = -A\tilde{C}_n + S \qquad \text{(V.B.4)}$$

where $\tilde{C}_n = (C_{n,1,1}(t), C_{n,1,2}(t), \ldots, C_{n,n,n}(t))$ and A and B are $n^2 x n^2$ matrices and S is an $n^2 x 1$ matrix. The matrices A and B consist of three bands, a tridiagonal band and two three-entry bands on either side of the diagonal, n entries from the diagonal.

The model uses the banded matrix routine given in von Rosenburg (44) to solve the system of linear equations resulting from Crank-Nicholson discretization of equation (V.B.4). Although this is an efficient Gaussian elimination routine, the storage requirements for direct solution of the $n^2 x n^2$ matrices are large. Hence, the model is limited to relatively few grid points. The model thus requires a more efficient use of storage than can be realized by the banded matrix routine. Such techniques as LSOR (31), or SIP (41), might be used to speed up the matrix inversion and reduce the storage requirements so that more grid points can be used.

# CHAPTER VI

## RESULTS FROM THE TWO-DIMENSIONAL FINITE ELEMENT MODEL

In Chapter IV acceptable bounds on the node spacing and time steps are given for the chapeau basis functions. It is desirable to find such a priori bounds for node spacing and time steps for the two-dimensional model so that acceptable accuracy is obtained for a given set of parameters. However, there are a number of parameters which can be varied: the pumping rate q, the dispersion coefficient, D, the well coordinates $(i_w, j_w)$, the constant unidirectional velocity $v_0$, and the length of the total field to be modeled, $\ell$. Thus, the question of appropriate node spacing and time steps is far more difficult for the two-dimensional model. For this model in particular, the problem is intensified by the fact that the number of nodes is limited by storage requirements for solving the linear system. These difficulties and how they can be overcome are included in the results to be given in this chapter.

### VI.A. The Well Equation

In Chapter II the two-dimensional convection-diffusion equation with simplifying assumptions is given by

$$D\left(\frac{\partial^2 C}{\partial x^2} + \frac{\partial^2 C}{\partial x^2}\right) - u_x \frac{\partial C}{\partial x} - u_y \frac{\partial C}{\partial y} = \Phi \frac{\partial C}{\partial t} + q(C_i - C) \qquad \text{(VI.A.1)}$$

Settari, Price, and Dupont (34) indicate that the source term, $q(C_i - C)$, is eliminated for a producing well because the produced concentration, $C_i$, is equal to the concentration, C, surrounding the well point. This suggests that no special conditions need to be provided for producing wells. Unfortunately, this does not prove to be the case.

Examination of the velocity vectors near the well indicate that how the vectors are evaluated is critical to the mass balance over the grid block surrounding the well point. The velocity vectors resulting from the analytical solution near the point sink have converging directions and the vector magnitudes increase without bound. Hence, the vector coordinates converge to both positive and negative infinity at the well point. To avoid this singularity, the well vector is assumed to be the average velocity in the grid block surrounding the well, which is equal to the constant unidirectional velocity, $v_0$. Evaluating the velocity vectors in this way produces unacceptable results from the model. As illustrated in Figure VI.A.1. the concentration tends to accumulate at the well and neighboring grid points. In this example, concentration values are computed for an 11 x 11 square grid. In the upper figure, the concentration at the well is graphed for each time step. The lower figure is a graph of the concentration values at five different time steps for the eleven grid points found in the line drawn from left to right through the well point. Since the normalized boundary concentration of 1.0 units represents a saturated concentration, values shown in the figure which are in excess of 1.0 are clearly in error. Apparently the model is not allowing for the mass to leave the system and hence, the contaminant accumulates at the well.

Equation (C4) in Appendix C suggests an alternative way to evaluate the velocities near the well point. Considering the velocity integral alone, it is apparent that only the nodes which are located at the well point or at the nearest neighboring grid points add to the velocity contribution for the equation at the well point. Similarly, the well point velocity vector enters into the equations for the nearest neighbor-

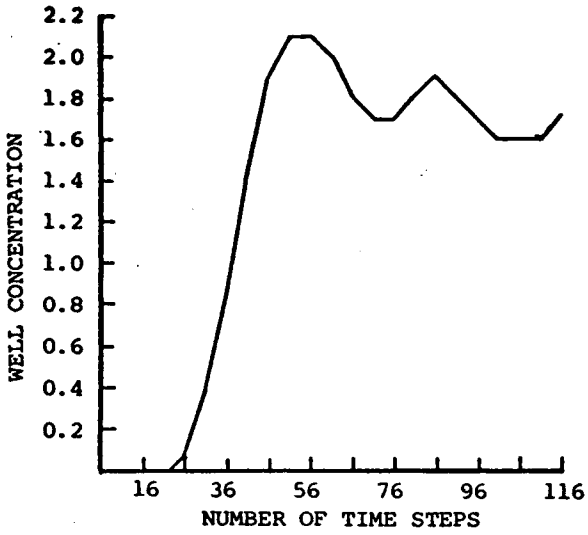


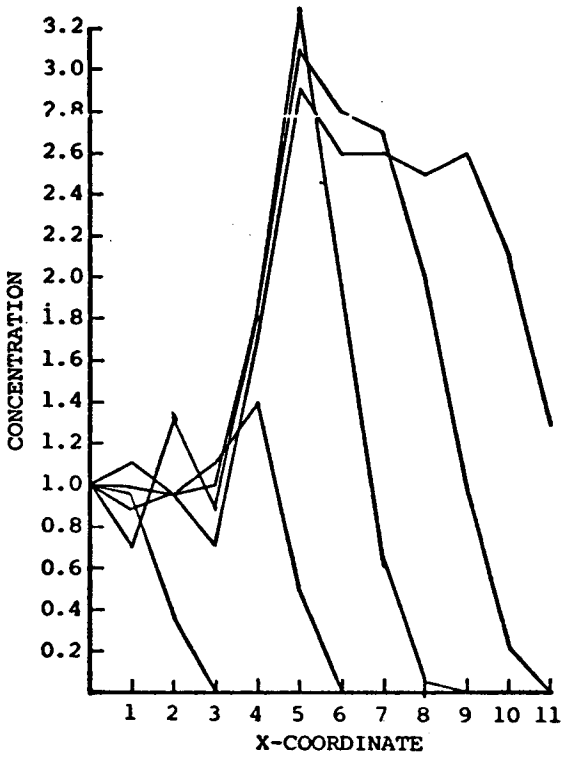


Figure VI.A.1. Results from the two-dimensional model with no special provisions for the equations near the well point.

ing points only. Since the velocity at the well point is not defined, it is desirable to evaluate the velocities at a finite radius from the well. This need only be done for the well point and its nearest neighbors. The remaining grid points in the model may use the velocity vectors computed at the grid points as described previously in Chapter V.

Evaluating the velocities in this way causes two types of changes in the equation for the nodes at and immediately adjacent to the well point. First, in the equation for a nearest neighboring grid point, the velocity vector for the well point is computed from the analytical solution at a finite radius from the well in the direction of the node point from the well. Thus, eight special velocities are computed for the well point velocity for the eight nearest neighbor equations. Second, for the equation of the well point itself, the integration of the well point velocity with the well point basis function is nonzero, unlike the remaining interior nodes in the model. In this case, the velocity coordinates evaluated at a finite radius are equal, but opposite in sign and when multiplied by the basis function derivative which also changes sign, the effect is to add a term to the well point equation for each of the four closest near neighboring points and for the well point itself. In other words, the typical integration of a grid point velocity with the basis function for the same grid point is zero:

$$u_x(i,j) \cdot \int_{(i-1)\Delta x}^{(i+1)\Delta x} w_i' w_i \, dx$$

$$= u_x(i,j)\left[ \int_{(i-1)\Delta x}^{i\Delta x} \frac{x-(i-1)\Delta x}{(\Delta x)^2} \, dx + \int_{i\Delta x}^{(i+1)\Delta x} \frac{(i+1)\Delta x - x}{(\Delta x)^2} \, dx \right]$$

$$= u_x(i,j)\cdot\left[\frac{(x-(i-1)\Delta x)^2}{2(\Delta x)^2}\Big|_{(i-1)\Delta x}^{i\Delta x} + \frac{((i+1)\Delta x-x)^2}{2(\Delta x)^2}\Big|_{i\Delta x}^{(i+1)\Delta x}\right]$$

$$= u_x(i,j)\cdot[(\tfrac{1}{2} - 0) + (0 - \tfrac{1}{2})]$$

$$= 0 \ ;$$

while evaluating the well point velocities at a finite radius produces a nonzero term:

$$u_x(i_w,j_w) \int_{(i_w-1)\Delta x}^{(i_w+1)\Delta x} w'_{i_w} w_{i_w}\, dx$$

$$= u_x(i_w,j_w)\left[\int_{(i_w-1)\Delta x}^{i_w\Delta x} \frac{x-(i-1)\Delta x}{(\Delta x)^2}\, dx + \int_{i\Delta x}^{(i+1)\Delta x} \frac{(i+1)\Delta x-x}{(\Delta x)^2} dx\right]$$

$$= u_x(i_w^-,j_w)\cdot[\tfrac{1}{2}] + u_x(i_w^+,j_w)\cdot[-\tfrac{1}{2}]$$

$$= (v_0 + \frac{q}{2\pi r})\cdot[\tfrac{1}{2}] + (v_0 - \frac{q}{2\pi r})\cdot[-\tfrac{1}{2}]$$

$$= \frac{q}{2\pi r} \qquad \text{(VI.A.3)}$$

where r is the chosen finite radius, $(i_w, j_w)$ is the well location, $i_w^- = i_w - r$ and $i_w^+ = i_w + r$.

By varying the choice of the radius r at which the velocities are to be evaluated, the concentrations calculated by the numerical solution vary from values too low at the well and too high at the nearest neighboring points, to values too high at the well and too low at the nearest neighboring points. The following analysis of the mass balance surrounding the well indicates a reasonable choice for r. The amount of

contaminant to be removed from the system is equal to the product of q, b, and C, where b is the aquifer thickness. The amount of contaminant entering the grid block surrounding the well is given by $[\bar{u}_x(i_w^-,j_w)+\bar{u}_x(i_w^+,j_w)+\bar{u}_y(i_w,j_w^-)+\bar{u}_y(i_w,j_w^+)]\cdot\Delta x\cdot b\cdot C$, where $\bar{u}$ is the average between the velocity evaluated at $\Delta x$ and the velocity at r. Hence, r must satisfy the following:

$$\left[\tfrac{1}{2}\left(v_0+\frac{q}{2\pi\Delta x}+v_0+\frac{q}{2\pi r}\right)+\tfrac{1}{2}\left(-v_o+\frac{q}{2\pi\Delta x}-v_o+\frac{q}{2\pi r}\right)\right.$$

$$\left.+\tfrac{1}{2}\left(\frac{q}{2\pi\Delta x}+\frac{q}{2\pi r}\right)+\tfrac{1}{2}\left(\frac{q}{2\pi\Delta x}+\frac{q}{2\pi r}\right)\right]\cdot\Delta x\cdot b\cdot C$$

$$= q\cdot b\cdot C$$

or $r_1 = \Delta x/(\pi-1)$ (VI.A.4)

The numerical results presented in the last section of this chapter use this radius for evaluating velocities near the well point.

Although not completely satisfactory, this technique tends to control the solution fairly well so that gross trends in the concentration profile can be evaluated. A further improvement might be gained by writing the dispersion coefficient as a function of the velocity as in Settari, Price, and Dupont (34). This would cause the dispersion coefficient to be higher near the well, therefore making the concentration profile less steep and easier to simulate numerically. A second refinement would be to write the analytical velocity functions inside the integrals and integrate the resulting smooth function. The inner integrals can be evaluated explicitly. The outer integrals can be evaluated using Gauss-Legendre guadrature. Such a refinement is not possible without collocation for non-steady-state problems or for difficult

geometries. However, comparing results from such a model with the model presented here would help to indicate the error involved in evaluating the velocities at the grid points only.

## VI.B. Determination of a Reasonable Time Step

An initial difficulty with the two-dimensional model concerned the choice of a suitable time step. For the first two geometries, the choice can be determined through use of an extension of equation (IV.B.1):

$$\Delta t_{max} = \Delta x/10\ \bar{u}_x \qquad \text{(VI.B.1)}$$

where $\bar{u}_x$ is the average of the x-coordinates of the velocity vectors. Reducing this time step size does not change the solution. Hence, this time step seems to be sufficiently small to prevent oscillations due to the time discretizations. In addition, results from the one-dimensional solution indicate how many time steps should be computed to provide answers over the time interval during which the relevant movement of the concentration profile was occuring. For the one-dimensional case, the dimensionless group $ut/\phi\ell$ measures how far the concentration value 0.5 has advanced as a fraction of the total field width, $\ell$. The dimensionless group $\bar{u}_x t/\phi\ell$ measures roughly how far across the two-dimensional field the concentration profile has advanced. Thus after m time steps, the concentration field has moved the fraction $\bar{u}_x m\Delta t/\phi\ell$ of the total field width $\ell = n\Delta x$. In the time interval of interest, the concentration profile moves from the left boundary to the value $\bar{u}_x t/\phi\ell = 1$. Hence the number of time steps required, for $\Delta t$ computed from equation (VI.B.1) is

$$m = \phi \ell / \bar{u}_x \Delta t$$

$$= \phi \ell / \bar{u}_x \cdot 10 \bar{u}_x / \phi \Delta x = 10\ell / \Delta x$$

$$= 10n$$

where n is the number of grid points. Using these criteria for $\Delta t$ and the number of time steps, the model will give results over a meaningful time interval.

VI.C. Test Results from the Two-Dimensional Model

One of the most difficult aspects of working with a two-dimensional model is determining whether the numerical results accurately represent the solution of the differential equation. When no analytical solution is available, the model designer must rely on comparisons with other numerical models, tests on whether the results from the same model differ when the spacing or time step size is reduced, and, in some cases, intuition about what should occur. Sometimes simplifying assumptions allow comparison with an analytical solution. Then when the model appears to work well for the simple case, more complicated features may be incorporated into the model.

The first tests for the model in this work was to compare with the one-dimensional analytical solution. On an 11x11 grid the model gives completely symmetric results which agree with the one-dimensional finite element solution using chapeau basis functions. Visible oscillations occur for $\lambda$ greater than 10n, as expected.

Velocity vectors computed by the model for a well producing at the rate of $10^{-3}$ cu.ft./sec./ft. located 2000 feet from the constant concentration boundary superimposed with a constant unidirectional velocity

equal to $10^{-6}$ ft./sec. are shown in Figure VI.C.1. The upper number in each pair is the x-coordinate of the velocity; the lower number is the y-coordinate. A positive x-coordinate indicates flow from left to right; a positive y-coordinate indicates flow from top to bottom. The coordinates are numbered starting from the upper left corner. Using this scheme, the well is located at the point $(i_w, j_w) = (4\Delta x, 6\Delta x)$. The analytical solution used to compute the velocity vectors is given by

$$u_x = v_o + \frac{q(x-i_x)}{2\pi r^2}, \quad u_y = \frac{q(y-j_w)}{2\pi r^2} \qquad \text{(VI.C.1)}$$

where $r^2 = (x-i_w)^2 + (y-j_w)^2$. The stagnation point occurs where $u_x = 0$, i.e. where $x = \frac{q}{2\pi v_0} + i_w$. In this case the stagnation point is less than one grid spacing to the right of the well point. For higher producing rates, the stagnation point moves further to the right of the well point resulting in some negative x velocity coordinates to the right of the well point.

Figures VI.C.2 and VI.C.3 show results from the two-dimensional convection-diffusion model using the velocity vectors in Figure VI.C.1 and dispersion coefficients of $10^{-4}$ and $10^{-5}$ ft.$^2$/sec., respectively. The porosity is equal to 0.3. Since the results are symmetric about a line drawn from left to right through the well point, the concentration values are contoured for the upper 11x6 grid points only. In the diagram at the top of the page, the contours marked "$\geq$ 1.0" mark the grid points farthest to the right which have concentrations greater than or equal to 1.0. Due to the oscillations in the solutions, there may be points to the left of these contours which have concentrations below 1.0. The remaining contours mark concentrations at the values indicated.

VELOCITY VECTORS

| | | | | | | | | | | |
|---|---|---|---|---|---|---|---|---|---|---|
| 0.10E-05 | 0.10E-05 | 0.10E-05 | 0.10E-05 | 0.99E-06 | 0.98E-06 | 0.97E-06 | 0.97E-06 | 0.97E-06 | 0.97E-06 | 0.97E-06 |
| 0.47E-07 | 0.55E-07 | 0.61E-07 | 0.64E-07 | 0.61E-07 | 0.55E-07 | 0.47E-07 | 0.39E-07 | 0.32E-07 | 0.26E-07 | 0.22E-07 |
| 0.10E-05 | 0.10E-05 | 0.10E-05 | 0.10E-05 | 0.98E-06 | 0.97E-06 | 0.96E-06 | 0.96E-06 | 0.96E-06 | 0.96E-06 | 0.97E-06 |
| 0.51E-07 | 0.64E-07 | 0.75E-07 | 0.80E-07 | 0.75E-07 | 0.64E-07 | 0.51E-07 | 0.40E-07 | 0.31E-07 | 0.24E-07 | 0.20E-07 |
| 0.11E-05 | 0.10E-05 | 0.10E-05 | 0.10E-05 | 0.97E-06 | 0.95E-06 | 0.95E-06 | 0.95E-06 | 0.95E-06 | 0.96E-06 | 0.96E-06 |
| 0.53E-07 | 0.73E-07 | 0.95E-07 | 0.11E-06 | 0.95E-07 | 0.73E-07 | 0.53E-07 | 0.38E-07 | 0.28E-07 | 0.21E-07 | 0.16E-07 |
| 0.11E-05 | 0.11E-05 | 0.11E-05 | 0.10E-05 | 0.94E-06 | 0.92E-06 | 0.93E-06 | 0.94E-06 | 0.95E-06 | 0.95E-06 | 0.96E-06 |
| 0.49E-07 | 0.80E-07 | 0.13E-06 | 0.16E-06 | 0.13E-06 | 0.80E-07 | 0.49E-07 | 0.32E-07 | 0.22E-07 | 0.16E-07 | 0.12E-07 |
| 0.11E-05 | 0.11E-05 | 0.12E-05 | 0.10E-05 | 0.84E-06 | 0.87E-06 | 0.90E-06 | 0.93E-06 | 0.94E-06 | 0.95E-06 | 0.96E-06 |
| 0.32E-07 | 0.64E-07 | 0.16E-06 | 0.32E-06 | 0.16E-06 | 0.64E-07 | 0.32E-07 | 0.19E-07 | 0.12E-07 | 0.86E-08 | 0.64E-08 |
| 0.11E-05 | 0.12E-05 | 0.13E-05 | 0.10E-05 | 0.68E-06 | 0.84E-06 | 0.89E-06 | 0.92E-06 | 0.94E-06 | 0.95E-06 | 0.95E-06 |
| 0. | 0. | 0. | 0. | 0. | 0. | 0. | 0. | 0. | 0. | 0. |
| 0.11E-05 | 0.11E-05 | 0.12E-05 | 0.10E-05 | 0.84E-06 | 0.87E-06 | 0.90E-06 | 0.93E-06 | 0.94E-06 | 0.95E-06 | 0.96E-06 |
| -0.32E-07 | -0.64E-07 | -0.16E-06 | -0.32E-06 | -0.16E-06 | -0.64E-07 | -0.32E-07 | -0.19E-07 | -0.12E-07 | -0.86E-08 | -0.64E-08 |
| 0.11E-05 | 0.11E-05 | 0.11E-05 | 0.10E-05 | 0.94E-06 | 0.92E-06 | 0.93E-06 | 0.94E-06 | 0.95E-06 | 0.95E-06 | 0.96E-06 |
| -0.49E-07 | -0.80E-07 | -0.13E-06 | -0.16E-06 | -0.13E-06 | -0.80E-07 | -0.49E-07 | -0.32E-07 | -0.22E-07 | -0.16E-07 | -0.12E-07 |
| 0.11E-05 | 0.10E-05 | 0.10E-05 | 0.10E-05 | 0.97E-06 | 0.95E-06 | 0.95E-06 | 0.95E-06 | 0.95E-06 | 0.96E-06 | 0.96E-06 |
| -0.53E-07 | -0.73E-07 | -0.95E-07 | -0.11E-06 | -0.95E-07 | -0.73E-07 | -0.53E-07 | -0.38E-07 | -0.28E-07 | -0.21E-07 | -0.16E-07 |
| 0.10E-05 | 0.10E-05 | 0.10E-05 | 0.10E-05 | 0.98E-06 | 0.97E-06 | 0.96E-06 | 0.96E-06 | 0.96E-06 | 0.96E-06 | 0.97E-06 |
| -0.51E-07 | -0.64E-07 | -0.75E-07 | -0.80E-07 | -0.75E-07 | -0.64E-07 | -0.51E-07 | -0.40E-07 | -0.31E-07 | -0.24E-07 | -0.20E-07 |
| 0.10E-05 | 0.10E-05 | 0.10E-05 | 0.10E-05 | 0.99E-06 | 0.98E-06 | 0.97E-06 | 0.97E-06 | 0.97E-06 | 0.97E-06 | 0.97E-06 |
| -0.47E-07 | -0.55E-07 | -0.61E-07 | -0.64E-07 | -0.61E-07 | -0.55E-07 | -0.47E-07 | -0.39E-07 | -0.32E-07 | -0.26E-07 | -0.22E-07 |

AVERAGE VELOCITY W-E = 0.9832E-06 LAMBDA = 0.5408E 03

Figure VI.C.1. Velocity vectors computed from the analytical solution for a point sink superimposed with a constant unidirectional velocity, $v_0 = 10^{-6}$ ft./sec.

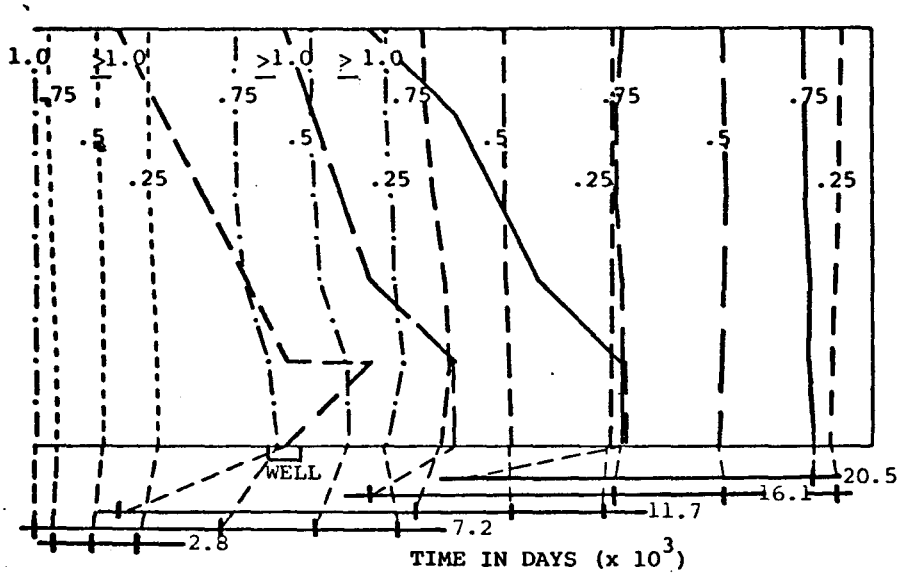


CONCENTRATION CONTOUR DIAGRAM

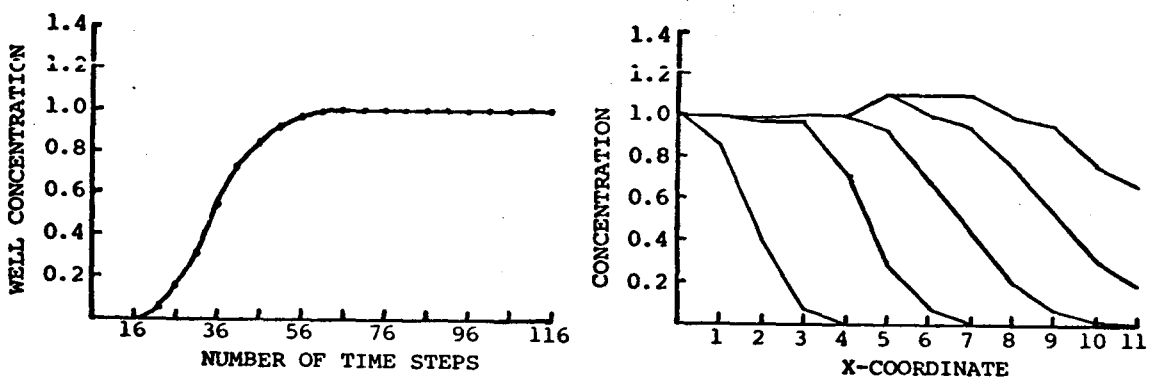


Figure VI.C.2. Results from the two-dimensional model for $\Delta x$ = 500 ft., $\Delta t = 1.526 \times 10^{7}$ sec., $v_0 = 10^{-6}$ ft./sec., q = .001 cu.ft./sec./ft. and $D = 10^{-4}$ ft.$^2$/sec., with well coordinates $(4\Delta x, 6\Delta x)$.

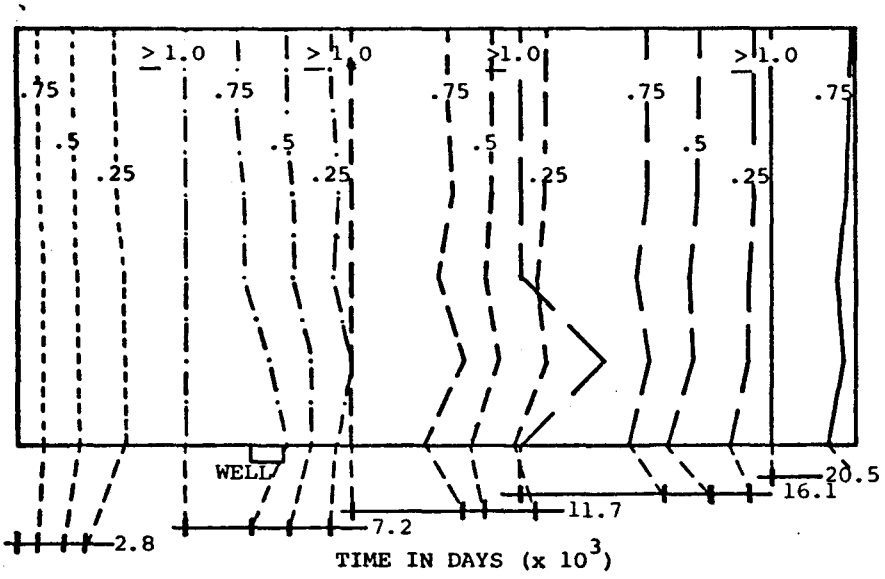


CONCENTRATION CONTOUR DIAGRAM

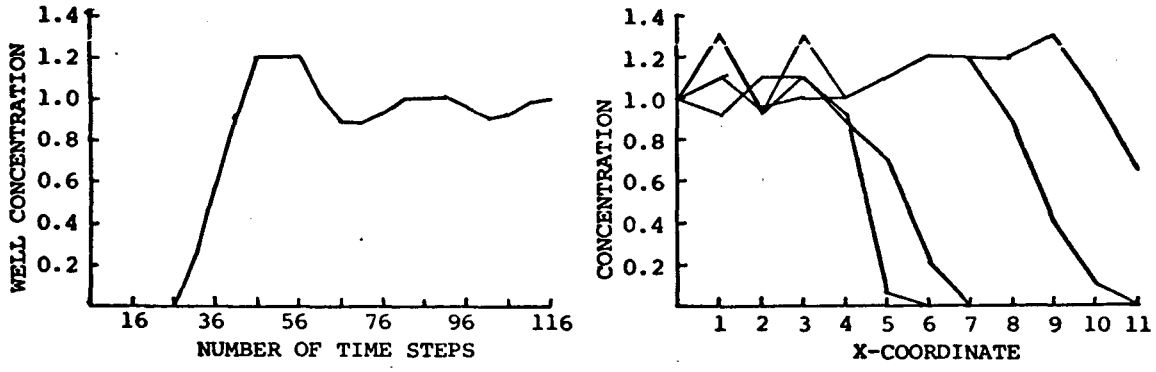


Figure VI.C.3. Results from the two-dimensional model for $\Delta x$ = 500 ft., $\Delta t = 1.526 \times 10^{7}$ sec., $v_0 = 10^{-6}$ ft./sec., q = .001 cu.ft./sec./ft., and $D = 10^{-5}$ ft.$^2$/sec., with well coordinates $(4\Delta x, 6\Delta x)$.

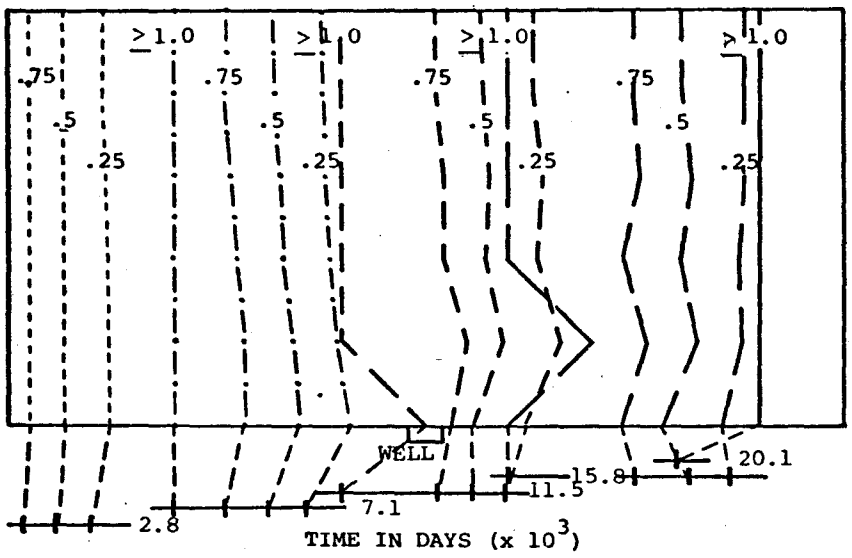


CONCENTRATION CONTOUR DIAGRAM

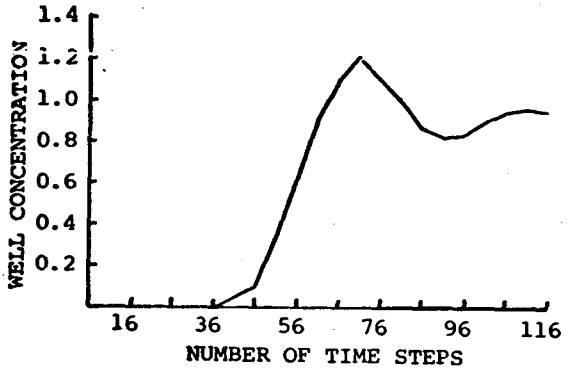


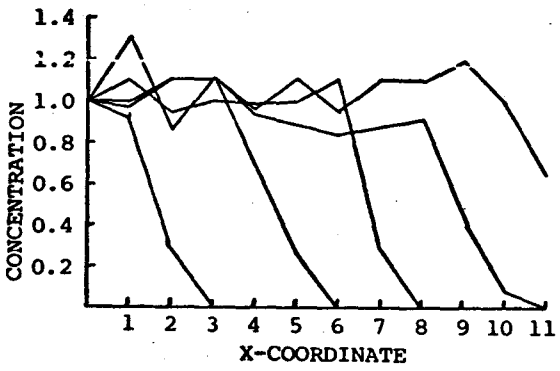


Figure VI.C.4. Results from the two-dimensional model for $\Delta x$ = 500 ft., $\Delta t = 1.5 \times 10^{7}$ sec., $v_0 = 10^{-6}$ ft./sec., q = .001 cu.ft./sec./ft., and $D = 10^{-5}$ ft.$^2$/sec., with well coordinate $(6\Delta x, 6\Delta x)$.

There are results from five time steps shown in each figure. The contours for each time step are drawn differently to distinguish the different times being presented. In addition, dashed lines connect each contour to a mark below the figure which represents the position of the same concentration value at the same time in the analytical solution computed for the unidirectional velocity, dispersion coefficient, and porosity used in the numerical model. The times shown on the contour diagram are indicated next to the appropriate analytical solution values.

The two graphs at the bottom of the page for each figure are intended to show the oscillations occuring in the solution. The lower left graph shows the concentration at the well point as a function of time. The lower right graph shows the concentrations computed for each time represented in the upper diagram for the grid points located on a line which passes from left to right through the well point. These two graphs reveal the oscillations about unity in the solution. Additional errors not shown in these graphs are the oscillations about zero which occur for several time steps early in time. These are always of small magnitude ($<10^{-1}$), and they disappear as the concentration values increase. The dispersion coefficients used in these two figures are several orders of magnitude larger than the dispersion coefficients for porous media given by Perkins and Johnston (  ). However, as revealed in the two figures, the oscillations increase significantly for a decrease in the dispersion coefficient from $10^{-4}$ ft.$^2$/sec. to $10^{-5}$ ft.$^2$/sec, and further decreases in the dispersion coefficient result in a solution that is of little value. The average velocity in the x-direction for these two figures is $9.8 \times 10^{-7}$ ft./sec. The Peclet number computed using

the average velocity is approximately 54 for Figure VI.C.2 and 540 for Figure VI.C.3. For Peclet numbers in the practical range, many more nodes would be required for this technique. Furthermore, if the constant velocity and/or the pumping rate is increased, even more nodes are required to control the oscillations in the solution.

Since the grid is fairly coarse, no effort has been made to smooth the contours or graphs of the results. However, even on such a coarse mesh, the trends in the results seem reasonable. The bending of the contours to the left of the well point toward the well shows the movement of the contaminant toward the well. The bending toward the well of the contours to the right of the well point show its effect on contaminant which is bypassing the well. Decreasing the dispersion coefficient causes a steeper concentration profile, as can be seen by comparing the two figures. In comparing with the marks representing the analytical solution, the expected result would be a "speeding up" of the concentration profile movement to the left of the well, but a "slowing down" of the movement after the front passes the well. This trend is reflected in the two figures.

Using the same format as described in the preceding paragraphs, Figure VI.C.4 shows results for the same parameters as in Figure VI.C.3, except for the position of the well point, which in this case is $(6\Delta x, 6\Delta x)$. Again, the same trends occur in the solution.

Results from the two-dimensional model are far less conclusive than for the one-dimensional model. Although predictions for suitable space and time steps based on the Peclet number computed using the average x velocity coordinate are fairly useful, increasing the spacing while

holding all other parameters at the same value increases the Peclet number, but the oscillations in the solution are reduced. A second result which occurred was that application of the time step condition given by equation (VI.B.1) to the third flow geometry produced undesirable results because the smaller velocities result in an unreasonably large time step. Such apparent contradictions in the results indicate that the complexity to the two-dimensional problem requires a more detailed description than can be provided by the simple dimensionless groups used in this work.

# CHAPTER VII

# CONCLUSIONS

In the first part of this work, five numerical models for the one-dimensional convection-diffusion equation are examined and compared to determine bounds on the space and time step sizes which limit numerical errors to within a specified tolerance. Each of the five methods exhibits one or both of the types of errors common to numerical solutions of convection-diffusion equations: oscillations about the correct solution and numerical dispersion. The following conclusions were drawn from numerical experiments using the models:

(1) For Peclet numbers the range from 0 to $10^3$ no significant oscillations due to the time discretization are introduced into solutions using any one of the five models tested if $\Delta\tau \leq 1/10\lambda n$.

(2) Using the above bound on the time step size, bounds on the space step which limit oscillations to less than 1.1 or 1.01 were found for the central difference approximation method and the finite element methods using chapeau basis functions and cubic Hermites.

(3) Both finite element methods required fewer modes than the central difference method to achieve the desired accuracy. The chapeau function method appears to be superior because of the weighted time discretization. The finite element method using cubic Hermites is a higher order approximation for the solution and, as expected, produces the most accurate results for a given space step size.

In developing the different models, a number of advantages and disadvantages for the methods were recognized. The finite difference methods were more straightforward to derive than the finite element

methods, but they are less accurate. Of the finite element methods, the chapeau functions are much easier to derive than the cubic Hermites because the integrations required are easier to perform, and there are fewer of them. In addition, the chapeau functions produce a simple tridiagonal system to solve, while the cubic Hermites require solution of a block diagonal matrix with six entries in each row. For the same number of linear equations, the cubic Hermites compute concentration values at half as many points as the remaining methods, because every other value computed is the derivative of the solution at a particular node. Hence, although cubic Hermites are more accurate, if a fine mesh is desired, a lower order method may be more appropriate.

The second objective of this work was to extend the finite element model using chapeau basis functions to two-dimensions. Preliminary results from the model lead to the following conclusions:

(1) The two-dimensional model when tested on a one-dimensional problem, agrees with the one-dimensional finite element model using chapeau basis functions when appropriate boundary conditions are imposed.

(2) Numerical results from the case of a producing well superimposed on a constant unidirectional velocity field indicate that special attention must be given to the equations at the well point and its nearest neighboring points. The method used in this work was to evaluate the velocities for the well point at a finite radius from the well. This technique appears to be fairly effective in providing for the mass to be removed from the system, but the somewhat arbitrary way in which the radius at which the velocities are evaluated is chosen suggests that further testing of this idea is desirable. One way to indicate the in-

fluence of the discreet evaluation of the velocities is to integrate the analytical velocity functions inside the basis function integrals. This would eliminate the need for evaluating the velocities near the well point differently from the remaining grid points.

(3) Requirements on the spacing and time step size limits are more difficult to acquire for the two-dimensional geometries, and the results thus far from the model are somewhat inclusive. A suitable time step for the flow geometries tested thus far appears to be given by a generalization for the one-dimensional result, $\Delta\tau \leq \Delta x/10u$, in which the average velocity is used in place of the constant velocity. The effect of varying the space step size was not adequately tested because of the expense involved in increasing the number of grid points.

(4) Numerical results for the flow pattern produced by a constant unidirectional velocity superimposed with a producing well were compared to the numerical results produced by the unidirectional velocity alone. Results from this comparison indicate that the higher velocities encountered near the well cause oscillations in in excess of the oscillations produced in the latter case. This observation, together with the necessity of calculating velocities at additional points not included in the model grid, suggests that a variable mesh might be advantageous.

(5) The coarse grid used was inadequate for handling dispersion coefficients in the practical range. If the one-dimensional results are any indication, for this scheme the number of grid points that would be required for more reasonable dispersion coefficients is prohibitive.

The rationale for choosing this particular technique for extending the chapeau basis functions to two-dimensions was that the development

of this technique is closely related to the derivation of the one-dimensional finite element model. The results from the model are somewhat encouraging, but a few improvements can be recommended. In particular, to allow for more grid points, a more efficient technique for solving the linear system is needed. This would allow more study on the effects of varying the space time size. Furthermore, integration of the analytical velocities would serve as a check on the technique of evaluating velocities at a finite radius from the well.

## REFERENCES


1. Bachmat, Y. and J. Bear, The general equations of hydrohynamic dispersion in homogeneous, isotropic, porous mediums, J. Geophys. Res., 69 (12), 2561-2567, 1964.

2. Bear, J., On the tensor form of dispersion in porous media, J. Geophys. Research, 66 (4), 1185-1197, 1961.

3. Blackwell, R.J., Laboratory studies of microscopic dispersion phenomena, Soc. Pet. Eng. J., March, p. 1, 1962.

4. Bredehoeft, J. D., Comment on ' Numerical solution to the convective diffusion equation' by C. A. Oster, J. C. Sonnichsen, and R. T. Jaske, Water Resour. Res., 7 (3), 755-756, 1971.

5. Bredehoeft, J. D. and G. F. Pinder, Mass transport in flowing groundwater, Water Resour. Res., 9 (1), 194-210, 1973.

6. Brigham, W.E., P.W. Reed, and J.N. Dew, Experiments on mixing during miscible displacement in porous media, Soc. Pet. Eng. J., March, p. 1, 1961.

7. Chaudhari, N. M., An improved numerical technique for solving multi-dimensional displacement equations, Soc. Pet. Eng. J., 11 (3), 277-284, 1971.

8. Chhatwal, S. S., An investigation of the centered-in-distance, centered-in-time method for solution of the convection-diffusion equation for liquid-liquid miscible displacement in porous media, Ph.D. dissertation, University of Kansas, Lawrence, Kansas, 1971.

9. Cleary, R. W. and D. D. Adrian, Analytical solution of the convective-dispersive equation, for cation adsorption in soils, Soil Science of America Proceedings, 37 (2), 197-199, 1973.

10. De Josselin de John, G. and M. J. Bossen, Discussion of paper by Jacob Bear, 'On the tensor form of dispersion in porous media', J. Geophys. Research, 66 (10), 3623-3624, 1961.

11. Fara, H. D. and A. E. Scheidegger, Statistical geometry of porous media, J. Geophys. Research, 66 (10), 3279-3284, 1961.

12. Gelhar, L. W. and M. A. Collins, General analysis of longitudinal dispersion in nonuniform flow, Water Resour. Res., 7 (6), 1511-1521, 1971.

13. Gray, W. G. and G. F. Pinder, An analysis of the numerical solution of the transport equation, Water Resour. Res., 12 (3), 547-555, 1976.

14. Guyman, G. L., A finite element solution of the one-dimensional diffusion-convection equation, Water Resour. Res., 6 (1), 204-210, 1970.

15. Guyman, G. L., V. H. Scott, and L. R. Herrmann, A general numerical solution of the two-dimensional diffusion-convection equation by the finite element method, Water Resour. Res., 6 (6), 1611-1617, 1970.

16. Huyakorn, P. and C. Taylor, Finite element models for coupled groundwater flow and convective dispersion, Proceedings from the International Conference on Finite Elements in Water Resources, Princeton University, July 1976.

17. Jacob, C. E., Flow of groundwater, Engineering Hydraulics, edited by H. Rouse, Chap. 5, John Wiley, New York, 1950.

18. Konikow, L. F. and J. D. Bredehoeft, Modeling flow and chemical quality changes in an irrigated stream-aquifer system, Water Resour. Res., 10 (3), 546-562, 1974.

19. Lantz, R. B., Quantitative evaluation of numerical diffusion (Truncation Error), Soc. Pet. Eng. J., 251 (Sept.), 315-320, 1971.

20. Laumbach, D. D., A high-accuracy finite-difference technique for the convection-diffusion equation, Soc. Pet. Eng. J., (Dec.), 517-531, 1975.

21. Lawson, D. W., Improvements in the finite difference solution of two-dimensional dispersion problems, Water Resour. Res., V (3), 721-725, 1971.

22. Nalluswami, M., R. A. Longenbaugh, and D. K. Sunada, Finite element method for the hydrohynamic dispersion equation with mixed partial derivatives, Water Resour. Res., 8 (5), 1247-1250, 1972.

23. Oster, C. A., J. C. Sonnichsen, and R. T. Jaske, Numerical solution to the convective diffusion equation, Water Resour. Res., 6 (6), 1746-1752, 1970.

24. Peaceman, D. W. and H. H. Rachford, Jr., Numerical calculation of multidimensional miscible displacement, Soc. Pet. Eng. J., (Dec.), 327-339, 1962.

25. Perkins, T. K. and O. C. Johnston, A review of diffusion and dispersion in porous media, Soc. Pet. Eng. J., (March), 70-84, 1963.

26. Pinder, G. F., A Galerkin-finite element simulation of groundwater contamination on Long Island, New York, Water Resour. Res., 9 (6), 1657-1669, 1973.

27. Pickens, J. F. and W. C. Lennox, Numerical simulation of waste movement in steady groundwater flow systems, Water Resour. Res., 12 (2), 171-179, 1976.

28. Price, H. S., J. C. Cavendish, and R. S. Varga, Numerical methods of higher-order accuracy for diffusion-convection equations, Soc. Pet. Eng. J., 243 (3), 293-303, 1968.

29. Price, H. S., R. S. Varga, and J. E. Warren, Applications of oscillation matrices to diffusion-convection equations, J. of Math. and Phys., 45 (Sept. ), 301-311, 1966.

30. Rachford, H. H., Jr., A sampling of variational methods, Proceedings, from the Fourth SPE Symposium on Numerical Simulation of Reservoir Performance, Los Angeles, California, Feb., 31-42, 1976.

31. Remson, I., G.M. Hornberger, and F.J. Molz, Numerical Methods in Subsurface Hydrology with an introduction to the finite element method, Wiley-Interscience, New York, 1971.

32. Scheidegger, A. E., General theory of dispersion in porous media, J. Geophys. Research, 66 (10), 3273-3278, 1961.

33. Scheidegger, Adrian E., Statistical hydrodynamics in porous media, J. Applied Phys., 25 (8), 994-1001, 1954.

34. Settari, A., H. S. Price, and T. Dupont, Development and application of variational methods for simulation of miscible displacement in porous media, Proceedings from the Fourth SPE Symposium on Numerical Simulation of Reservoir Performance, Los Angeles, California, Feb., 43-68, 1976.

35. Shamir, U. Y. and D. R. F. Harleman, Numerical solutions for dispersion in porous mediums, Water Resour. Res., 3 (2), 557-581, 1967.

36. Smith, I. M., Integration in time of diffusion and diffusion-convection equations, Proceedings from the International Conference on Finite Elements in Water Resources, Princeton University, July, 1976.

37. Smith, I. M., R. V. Farraday, and B. A. O'Connor, Rayleigh-Ritz and Galerkin finite elements for diffusion-convection problems, Water Resour. Res., 9 (3), 593-606, 1973.

38. Stone, H. L., Iterative solutions of implicit approximations of multi-dimensional partial differential equations, SIAM J. on Numerical Analysis, V. 5, p. 530, 1968.

39. Stone, H. L., and P. L. T. Brian, Numerical solution of convective transport problems, A. I. Ch. E. Journal, 9 (5), 681-688, 1963.

40. Warren, J. E. and F. F. Skiba, Macroscopic dispersion, Soc. Pet. Eng. J., (Sept.), 215-229, 1964.

41. Weinstein, H. G., H. L. Stone, and T. V. Kwan, Iterative procedure for solution of systems of parabolic and elliptic equations in three dimensions, Ind. and Eng. Chem. Fundamentals, V. 8, May, p. 282, 1969.

42. Weinstein, H. G., H. L. Stone, and T. V. Kwan, Simultaneous solution of multiphase reservoir flow problems, Soc. Pet. Eng. J., June, p. 99, 1970.

43. Van Genuchten, M. Th., On the accuracy and efficiency of several numerical schemes for solving the convective-dispersive equation, Proceedings from the International Conference on Finite Elements in Water Resources, Princeton University, July, 1976.

44. Von Rosenberg, D.V., Methods for the Numerical Solution of Partial Differential Equations, American Elsevier Publishing Company, Inc., New York, 1969.

## APPENDIX A

## DERIVATIONS OF FINITE DIFFERENCE FORMULAS

Several finite difference formulas can be derived from the following Taylor series expansions:

$$f_{i-2} = f_i - f_i'(2h) + f_i''\frac{(2h)^2}{2} - f_i'''\frac{(2h)^3}{6} + O(h^4) \quad \text{(A1)}$$

$$f_{i-1} = f_i - f_i'h + f_i''\frac{h^2}{2} - f_i'''\frac{h^3}{6} + O(h^4) \quad \text{(A2)}$$

$$f_{i+1} = f_i + f_i'h + f_i''\frac{h^2}{2} - f_i'''\frac{h^3}{6} + O(h^4) \quad \text{(A3)}$$

where $f_i = f(ih)$

1. Backward Difference

Rearrange equation (A2) to give

$$f_i' = \frac{f_i - f_{i-1}}{h} + O(h) \quad \text{(A4)}$$

2. Foreward Difference

Rearrange equation (A3) to give

$$f_i' = \frac{f_{i+1} - f_i}{h} + O(h) \quad \text{(A5)}$$

3. Central Difference

Subtract equation (A2) from (A3) to give

$$f_i' = \frac{f_{i+1} - f_{i-1}}{2h} + O(h^2) \quad \text{(A6)}$$

4. Three Point Backward Difference

Subtract 4 x equation (A2) from equation (A1) to give

$$f_i' = \frac{f_{i-2} - 4f_{i-1} + 3f_i}{2h} + O(h^2) \quad \text{(A7)}$$

5. Second Derivative

Add equation (A2) to (A3) to give

$$f_i'' = \frac{f_{i-1} - 2f_i + f_{i+1}}{h^2} + O(h^2) \quad \text{(A8)}$$

## APPENDIX B

## NUMERICAL METHODS FOR SOLVING THE ONE-DIMENSIONAL CONVECTION-DIFFUSION EQUATION

Five numerical methods for solving the one-dimensional convection-diffusion equation are compared in this work. The convection-diffusion equation in dimensionless variables is given by

$$\frac{\partial c}{\partial t}(x,t) = \frac{\partial^2 c}{\partial x^2}(x,t) - \lambda\frac{\partial c}{\partial x}(x,t) \ , \quad 0 < x \leq 1 \ , \quad t > 0 \tag{B1}$$

with boundary and initial conditions given by

$$\begin{aligned} &c(0,t) = 1 \ , \quad t > 0 \\ &\frac{\partial c}{\partial x}(1,t) = 0 \ , \quad t > 0 \\ &c(x,0) = 0 \ , \quad 0 < x \leq 1 \end{aligned} \tag{B2}$$

For a uniform mesh $h = 1/n$ ($2/n$ for cubic Hermites), the spacial discretization of equations (B1) and (B2) results in a system of ordinary differential equations which is represented by

$$B\frac{d\tilde{c}}{dt}(t) = -A\tilde{c}(t) + S \tag{B3}$$

where $\tilde{c}(t) = (c(h,t), c(2h,t), \ldots, c(1,t))$. The matrices A and B (nxn) and S (nx1) are developed below for each of the five methods.

### 1. Central Difference Approximation

The central difference approximation uses the second order correct approximations for the derivatives in the diffusion and convection terms given by equations (A8) and (A6), respectively. Thus, equation (B1) is approximated by

$$\begin{aligned} \frac{dc_i}{dt} &= \frac{1}{h^2}(c_{i-1} - 2c_i + c_{i+1}) - \frac{\lambda}{2h}(c_{i+1} - c_i) \\ &= \frac{1}{h^2}[(1+\lambda h/2)c_{i-1} - 2c_i + (1-\lambda h/2)c_{i+1}] \ , \quad 1 \leq i \leq n-1 \end{aligned} \tag{B4}$$

where $c_i = c(ih,t)$. Equations (B2) are given by

$$c_0 = 1 \ , \ t > 0$$

$$\frac{c_{n+1} - c_{n-1}}{2h} = 0 \ , \ t > 0 \tag{B5}$$

$$c_i = 0 \ , \ 1 \leq i \leq n \ , \ t = 0$$

The second equation (B5) together with equation (B4) determine the $n^{th}$ equation

$$\frac{dc_n}{dt} = \frac{2c_{n-1} - 2c_n}{h^2} \tag{B6}$$

Hence, the matrices A, B, and S are given by the following:

$$A = \begin{bmatrix} 2 & -(1-\alpha) & & & \\ -(1+\alpha) & 2 & -(1-\alpha) & & \\ & -(1+\alpha) & 2 & -(1-\alpha) & \\ & & -2 & 2 & \end{bmatrix} \cdot \frac{1}{h^2} \tag{B7}$$

$$B = \begin{bmatrix} 1 & & \\ & \ddots & \\ & & 1 \end{bmatrix} \tag{B8}$$

$$S = \begin{bmatrix} 1+\alpha \\ 0 \\ \cdot \\ \cdot \\ \cdot \\ 0 \end{bmatrix} \cdot \frac{1}{h^2} \tag{B9}$$

where $\alpha = \lambda h/2$.

## 2. Non-Central Difference Approximation

The non-central difference approximation given by Price, Varga, and Warren uses the three point backward difference equation given by equation (A7) for nodes $2 \leq i \leq n-1$. The equation for node 1 uses the foreward difference formula given by equation (A5), and the equation for node n uses the central difference approximation as described for the CDA method. Equation (B1) is approximated by the following n ordinary differential equations:

$$\frac{dc_1}{dt} = \frac{1}{h^2}[-(2+\lambda h)c_1 + c_2 + (1+\lambda h)c_0]$$

$$\frac{dc_i}{dt} = \frac{1}{h^2}[-(\frac{\lambda h}{2})c_{i-2} + (1+2\lambda h)c_{i-1} - (2+\frac{3\lambda h}{2})c_i + c_{i+1}] \ , \quad 2 \leq i \leq n-1$$

$$\frac{dc_n}{dt} = \frac{1}{h^2}[2c_{n-1} - 2c_n] \qquad \text{(B10)}$$

The matrix B is the identity matrix as in the CDA method. The matrices A and S are given below:

$$A = \begin{bmatrix} 2+\lambda h & 1 & & & & \\ -(1+2\lambda h) & -(2+\frac{3\lambda h}{2}) & 1 & & & \\ \frac{\lambda h}{2} & -(1+2\lambda h) & -(2+\frac{3\lambda h}{2}) & 1 & & \\ & \ddots & \ddots & \ddots & \ddots & \\ & & \frac{\lambda h}{2} & -(1+2\lambda h) & -(2+\frac{3\lambda h}{2}) & 1 \\ & & & & -2 & 2 \end{bmatrix} \cdot \frac{1}{h^2} \qquad \text{(B11)}$$

$$S = \begin{bmatrix} 1+\lambda h \\ \frac{\lambda h}{2} \\ 0 \\ \cdot \\ \cdot \\ \cdot \\ 0 \end{bmatrix} \cdot \frac{1}{h^2} \qquad \text{(B12)}$$

3. Finite Element with Chapeau Basis Functions

The derivation given here is described in Price, Cavendish, and Varga ( ).

Let $c_n(x,t)$ be an approximation for $c(x,t)$ defined by

$$c_n(x,t) = \sum_{k=1}^{n} c_{n,k}(t)w_k(x) + w_0(x) \qquad \text{(B13)}$$

where $\{w_1(x), w_2(x), \ldots, w_n(x)\}$ span the subspace $S_n$ of S, the set of all real-valued piecewise continuously differentiable functions $w(x)$ on the interval $[0,1]$ such that $w(0) = 0$, $\frac{dw}{dx}(1) = 0$, and $w_0(0) = 1$, $\frac{dw_o}{dx}(1) = 0$. The coefficients $c_{n,k}(t)$ are determined by the following:

$$\int_0^1 ( \frac{\partial c_n}{\partial t} - \frac{\partial^2 c_n}{\partial x^2} + \lambda \frac{\partial c_n}{\partial x} ) \ w_k(x) \ dx = 0 \ , \quad 1 \leq k \leq n, \ t > 0 \qquad \text{(B14)}$$

and $\| w_0(x) + \sum_{k=1}^{n} c_{n,k}(0) w_k(x) \|_{L^2} = \min_{\alpha_i} \| w_0(x) + \sum_{k=1}^{n} \alpha_k w_k(x) \|_{L^2}$ (B15)

where $\| f(x) \|_{L^2} = \int_{-\infty}^{\infty} [f(x)]^2 dx$

Equation (B14) is an integrated form over the space $S_n$ of equation (B1), and equation (B15) is a least squares approximation to the initial conditions.

Equation (B14) is simplified with the following steps:

$$0 = \int_0^1 \left( \frac{\partial c_n}{\partial t} - \frac{\partial^2 c_n}{\partial x^2} + \lambda \frac{\partial c_n}{\partial x} \right) w_k dx$$

$$= \int_0^1 \left( \sum_{j=1}^{n} \frac{dc_{n,j}}{dt} w_j \right) w_k dx - \int_0^1 \left( \sum_{j=1}^{n} c_{n,j} \frac{d^2 w_j}{dx^2} \right) w_k dx$$

$$+ \lambda \int_0^1 \left( \sum_{j=1}^{n} c_{n,j} \frac{dw_j}{dx} \right) w_k dx - \int_0^1 \frac{d^2 w_0}{dx^2} w_k dx + \lambda \int_0^1 \frac{dw_0}{dx} w_k dx$$

$$= \sum_{j=1}^{n} c'_{n,j} \int_0^1 w_j w_k dx - \sum_{j=1}^{n} c_{n,j} \int_0^1 w''_j w_k dx + \lambda \sum_{j=1}^{n} c_{n,j} \int_0^1 w'_j w_k dx$$

$$- \int_0^1 w''_0 w_k dx + \lambda \int_0^1 w'_0 w_k dx$$

$$= \dagger \sum_{j=1}^{n} c'_{n,j} \int_0^1 w_j w_k dx - \sum_{j=1}^{n} c_{n,j} \left( w'_j(1) w_k(1) - w'_j(0) w_k(0) - \int_0^1 w'_j w'_k dx \right)$$

$$+ \lambda \sum_{j=1}^{n} c_{n,j} \int_0^1 w'_j w_k dx - w'_0(1) w_k(1) + w'_0(0) w_k(0) + \int_0^1 w'_0 w'_k dx$$

$$+ \lambda \int_0^1 w'_o w_k dx$$

$$= \sum_{j=1}^{n} c'_{n,j} \int_0^1 w_j w_k dx + \sum_{j=1}^{n} c_{n,j} \int_0^1 (w'_j w'_k + \lambda w'_j w_k) dx$$

$$+ \int_0^1 (w'_0 w'_k + \lambda w'_0 w_k) dx , \quad 1 \leq k \leq n , \quad t > 0$$

† with rearrangement and integration by parts

or

$$\begin{bmatrix} \int_0^1 w_1 w_1 dx & \cdots & \int_0^1 w_n w_1 dx \\ \vdots & & \vdots \\ \int_0^1 w_1 w_n dx & \cdots & \int_0^1 w_n w_n dx \end{bmatrix} \cdot \begin{bmatrix} c'_{n,1} \\ \vdots \\ c'_{n,n} \end{bmatrix}$$

$$+ \begin{bmatrix} \int_0^1 (w'_1 w'_1 + \lambda w'_1 w_1) dx & \cdots & \int_0^1 (w'_n w'_1 + \lambda w'_n w_1) dx \\ \vdots & & \vdots \\ \int_0^1 (w'_1 w'_n + \lambda w'_1 w_n) dx & \cdots & \int_0^1 (w'_n w'_n + \lambda w'_n w_n) dx \end{bmatrix} \cdot \begin{bmatrix} c_{n,1} \\ \vdots \\ c_{n,n} \end{bmatrix}$$

$$= - \begin{bmatrix} \int_0^1 (w'_0 w'_1 + \lambda w'_0 w_1) dx \\ \vdots \\ \int_0^1 (w'_0 w'_n + \lambda w'_0 w_n) dx \end{bmatrix} \qquad \text{(B16)}$$

The matrix multiplying $\tilde{c}'_n$ is B, the matrix multiplying $\tilde{c}_n$ is A, and the matrix on the right-hand side of equation (B16) is S. After basis functions are supplied, the integrals can be evaluated as will be shown below.

The norm on the right-hand side of equation (A15) is minimized when

$$0 = \frac{\partial}{\partial x_i} \left\| w_0 + \sum_{k=1}^{n} \alpha_k w_k \right\|_{L^2} = \frac{\partial}{\partial x_i} \int_0^1 (w_0 + \sum_{k=1}^{n} \alpha_k w_k)^2 dx$$

$$= \frac{\partial}{\partial x_i} \int_0^1 (w_0^2 + 2w_0 \sum_{k=1}^{n} \alpha_k w_k + \sum_{k=1}^{n} \sum_{l=1}^{n} \alpha_k w_k \alpha_l w_l) dx$$

$$= 2 \int_0^1 (w_0 w_i + \sum_{k=1}^{n} \alpha_k w_k w_i) dx \; ; \quad 1 \leq i \leq n \qquad \text{(B17)}$$

or

$$A\tilde{c}_n = -\begin{bmatrix} \int_0^1 w_0 w_1 dx \\ \vdots \\ \int_0^1 w_0 w_n dx \end{bmatrix}$$

with A defined as above.

As in Price, Cavendish, and Varga ( ), the chapeau basis functions $w_1(x),\ldots,w_n(x)$, and $w_0(x)$ are defined to be the following:

$$w_0(x) = \begin{cases} -(x-h)/h, & 0 \le x \le h \\ 0, & h \le x \le 1 \end{cases}$$

$$w_1(x) = \begin{cases} (x-(i-1)h)/h, & (i-1)h \le x \le ih \\ ((i+1)h-x)/h, & ih \le x \le (i+1)h, \quad 1 \le i \le n-2 \\ 0, & \text{elsewhere} \end{cases}$$

$$w_{n-1}(x) = \begin{cases} (x-(n-2)h)/h, & (n-2)h \le x \le (n-1)h \\ (nh-x)^2/h^2, & (n-1)h \le x \le nh = 1 \\ 0, & 0 \le x \le (n-2)h \end{cases}$$

$$w_n(x) = \begin{cases} -((x-nh)^2-h^2)/h^2, & (n-1)h \le x \le nh = 1 \\ 0, & 0 \le x \le (n-1)h \end{cases} \qquad \text{(B18)}$$

where $w_{n-1}(x)$ and $w_n(x)$ are piecewise-quadratic basis functions to provide for the zero derivative on the right-hand boundary. The chapeau basis functions are illustrated in the figure below:

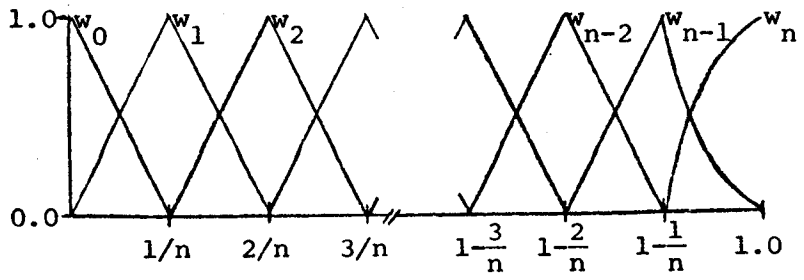

Performing the integrations in equation (B16) for the chapeau basis functions defined above leads to the following matrices for A, B, and S.

$$A = \begin{bmatrix} 2 & -(1-\alpha) & & \\ -(1+\alpha) & 2 & -(1-\alpha) & \\ & -(1+\alpha) & \frac{7}{3} & -(\frac{4}{3}-\alpha) \\ & & -(\frac{4}{3}+\alpha) & (\frac{4}{3}+\alpha) \end{bmatrix} \cdot \frac{1}{h} \tag{B19}$$

$$B = \begin{bmatrix} \frac{2}{3} & \frac{1}{6} & & \\ \frac{1}{6} & \frac{2}{3} & \frac{1}{6} & \\ & \frac{1}{6} & \frac{8}{15} & \frac{2}{15} \\ & & \frac{2}{15} & \frac{8}{15} \end{bmatrix} \cdot h \tag{B20}$$

$$S = \begin{bmatrix} 1+\alpha \\ 0 \\ \cdot \\ \cdot \\ \cdot \\ 0 \end{bmatrix} \cdot \frac{1}{h} \tag{B21}$$

where $\alpha = \lambda h/2$

If chapeau basis functions are used throughout with no quadratic boundary functions, then matrices A and B become the following:

$$A = \begin{bmatrix} 2 & -(1-\alpha) & & \\ -(1+\alpha) & 2 & -(1-\alpha) & \\ & -(1+\alpha) & 2 & -(1-\alpha) \\ & & -(1+\alpha) & (1+\alpha) \end{bmatrix} \cdot \frac{1}{h} \tag{B22}$$

$$B = \begin{bmatrix} \frac{2}{3} & \frac{1}{6} & & \\ \frac{1}{6} & \frac{2}{3} & \frac{1}{6} & \\ & \frac{1}{6} & \frac{2}{3} & \frac{1}{6} \\ & & \frac{1}{6} & \frac{1}{3} \end{bmatrix} \cdot h \tag{B23}$$

## 4. Finite Element with Cubic Hermite Bases Functions

The derivation of the matrices A, B, and S for the finite element method using cubic Hermite basis functions is analogous to the derivation for the chapeau basis functions. Price, Cavendish, and Varga define the cubic Hermite basis functions on n/2 mesh intervals of length h as the following:

$$w_0(x) = \begin{cases} (2x+h)(x-h)^2/h^3 & , \quad 0 \le x \le h \\ 0 & , \quad h \le x \le 1 \end{cases}$$

$$w_1(x) = \begin{cases} x(x-h)^2/h^2 & , \quad 0 \le x \le h \\ 0 & , \quad h \le x \le 1 \end{cases}$$

$$w_{2i}(x) = \begin{cases} (-2x+(1+2i)h)(x-(i-1)h)^2/h^3 & , \quad (i-1)h \le x \le ih \\ (2x+(1-2i)h)(x-(i+1)h)^2/h^3 & , \quad ih \le x \le (i+1)h \ , \\ & \quad 1 \le i \le n/2-1 \\ 0 & , \quad \text{elsewhere} \end{cases}$$

$$w_{2i+1}(x) = \begin{cases} (x-ih)(x-(i-1)h)^2/h^2 & , \quad (i-1)h \le x \le ih \\ (x+ih)(x-(i+1)h)^2/h^2 & , \quad ih \le x \le (i+1)h \ , \\ & \quad 1 \le i \le n/2-1 \\ 0 & , \quad \text{elsewhere} \end{cases}$$

$$w_n(x) = \begin{cases} (2x+(1+n)h)(x-(n/2-1)h)^2/h^3 & , \quad (n/2-1)h \le x \le 1 \\ 0 & , \quad \text{elsewhere} \end{cases} \qquad \text{(B24)}$$

The cubic Hermite basis functions are illustrated below:

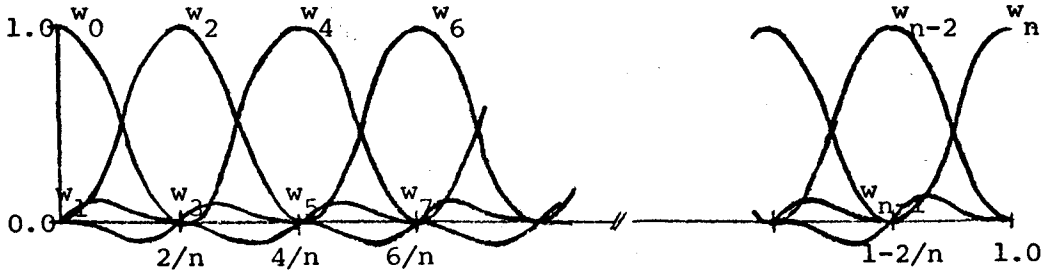

Notice that the cubic Hermite functions are piecewise-cubic polynomials which have continuous first derivatives. Performing the integrations in equation (B16) for cubic Hermite basis functions leads to the following matrices:

$$B = \begin{bmatrix} \frac{h^3}{105} & \frac{13h^2}{420} & \frac{-5h^3}{700} & & & & & & & & & \\ \frac{13h^2}{420} & \frac{26h}{35} & 0 & \frac{9h}{70} & \frac{-13h^2}{420} & & & & & & & \\ \frac{-5h^3}{700} & 0 & \frac{2h^3}{105} & \frac{13h^2}{420} & \frac{-5h^2}{700} & & & & & & & \\ & & & \frac{9h}{70} & \frac{13h^2}{420} & \frac{26h}{35} & 0 & \frac{9h}{70} & \frac{-13h^2}{420} & & & \\ & & & \frac{-13h^2}{420} & \frac{-5h^3}{700} & 0 & \frac{2h^3}{105} & \frac{13h^2}{420} & \frac{-5h^3}{700} & & & \\ & & & & & & \frac{9h}{70} & \frac{13h^2}{420} & \frac{26h}{35} & 0 & \frac{9h}{70} & \frac{-13h^2}{420} \\ & & & & & & \frac{-13h^2}{420} & \frac{-5h^3}{700} & 0 & \frac{2h^3}{105} & \frac{13h^2}{420} & \frac{-5h^3}{700} \\ & & & & & & & & \frac{9h}{70} & \frac{13h^2}{420} & \frac{26h}{35} & 0 & \frac{9h}{70} \\ & & & & & & & & \frac{-13h^2}{420} & \frac{-5h^3}{700} & 0 & \frac{2h^3}{105} & \frac{13h^2}{420} \\ & & & & & & & & & & \frac{9h}{70} & \frac{13h^2}{420} & \frac{13h}{35} \end{bmatrix} \quad \text{(B25)}$$

$$S = \begin{bmatrix} \frac{-(1-\lambda h)}{10} \\ \frac{6}{5h} + \frac{\lambda}{2} \\ \frac{-(1+\lambda h)}{10} \\ 0 \\ \cdot \\ \cdot \\ \cdot \\ 0 \end{bmatrix} \quad \text{(B26)}$$

$$A = -\begin{bmatrix} \dagger\dagger & \frac{-(1-\lambda h)}{10} & \frac{-h(2+\lambda h)}{60} & & & & \\ \frac{-(1+\lambda h)}{10} & \frac{12}{5h} & \frac{\lambda h}{15} & \frac{-6}{5h}+\frac{\lambda}{2} & \frac{(1-\lambda h)}{10} & & \\ \frac{-h(2-\lambda h)}{60} & \frac{-\lambda h}{5} & \frac{4h}{15} & \frac{-(1-\lambda h)}{10} & \frac{-h(2+\lambda h)}{60} & & \\ & \frac{-6}{5h}-\frac{\lambda}{2} & \frac{-(1+\lambda h)}{10} & \frac{12}{5h} & \frac{\lambda h}{5} & \frac{-6}{5h}+\frac{\lambda}{2} & \frac{(1-\lambda h)}{10} \\ & \frac{(1+\lambda h)}{10} & \frac{-h(2-\lambda h)}{60} & \frac{-\lambda h}{5} & \frac{4h}{15} & \frac{-(1-\lambda h)}{10} & \frac{-h(2+\lambda h)}{60} \end{bmatrix}$$

$$\begin{bmatrix} \frac{-6}{5h}-\frac{\lambda}{2} & \frac{-(1+\lambda h)}{10} & \frac{12}{5h} & \frac{\lambda h}{5} & \frac{-6}{5h}+\frac{\lambda}{2} & \frac{(1-\lambda h)}{10} & \\ \frac{(1+\lambda h)}{10} & \frac{-h(2-\lambda h)}{60} & \frac{-\lambda h}{5} & \frac{4h}{15} & \frac{-(1-\lambda h)}{10} & \frac{-h(2+\lambda h)}{60} & \\ & \frac{-6}{5h}-\frac{\lambda}{2} & \frac{-(1+\lambda h)}{10} & \frac{12}{5h} & \frac{\lambda h}{5} & \frac{-6}{5h}+\frac{\lambda}{2} & \\ & \frac{(1+\lambda h)}{10} & \frac{-h(2-\lambda h)}{60} & \frac{-\lambda h}{5} & \frac{4h}{15} & \frac{-(1-\lambda h)}{10} & \\ & & \frac{-6}{5h}-\frac{\lambda}{2} & \frac{-(1+\lambda h)}{10} & \frac{6}{5h}+\frac{\lambda}{2} & & \end{bmatrix}$$

$$\dagger\dagger = \frac{2h}{15} - .6345 \times 10^{-17}\lambda h^2 \qquad \text{(B27)}$$

## 5. Lumped Matrix Approximation

The lumped matrix approximation used in this work is identical to the finite element method using chapeau basis functions except that the matrix B which multiplies the time derivative is replaced by the identity matrix.

## APPENDIX C

## TWO-DIMENSIONAL FINITE ELEMENT MODEL USING CHAPEAU BASIS FUNCTIONS

Let $c_n(x,y,t)$ be an approximation for the solution $c(x,y,t)$ of equation (II.A.6) defined by

$$c_n(x,y,t) = \sum_{k=1}^{n}\sum_{l=1}^{n} c_{n,k,l}(t)w_k(x)w_l(y) + w_\partial(x)\tilde{w}_\partial(y) \qquad (C1)$$

where $w_1(x), w_2(x), \ldots, w_n(x)$, $\tilde{w}_1(y), \tilde{w}_2(y), \ldots, \tilde{w}_n(y)$, $w_\partial(x), \tilde{w}_\partial(y)$ are piecewise-linear polynomials defined over the region F with appropriate conditions of the boundary of F, $\partial F$, and the functions $w_\partial(x)$ and $\tilde{w}_\partial(y)$ provide for nonzero boundary conditions. The coefficients $c_{n,k,l}(t)$ are determined by the following:

$$\iint_F \left[\left(\Phi\frac{\partial}{\partial t}c_{n,i,j} - D\left(\frac{\partial^2 c}{\partial x^2} + \frac{\partial^2 c}{\partial y^2}\right)_{n,i,j} + \left(u_x\frac{\partial c}{\partial x} + u_y\frac{\partial c}{\partial y}\right)_{n,i,j}\right) \cdot w_k(x)dx\right]\tilde{w}_l(y)dy = 0 \; ; \quad 1 \le k,l \le n \; , \quad 1 \le i,j \le n \qquad (C2)$$

and $$\left\| c_n(x,y,0) \right\|_{L^2[F]} = \min_{\alpha_{i,j}} \left\| \sum_{k=1}^{n}\sum_{l=1}^{n} \alpha_{i,j}w_k(x)\tilde{w}_l(y) + w_\partial(x)\tilde{w}_\partial(y) \right\|_{L^2[F]} \qquad (C3)$$

Equations (C2) and (C3) are analogous to equations (B14) and (B15), respectively.

The integral in equation (C2) is simplified according to the following steps:

$$0 = \Phi\iint_F \sum_{i=1}^{n}\sum_{j=1}^{n} c'_{n,i,j}w_i\tilde{w}_j w_k\tilde{w}_l dxdy$$

$$- D\iint_F \sum_{i=1}^{n}\sum_{j=1}^{n} c_{n,i,j}(w'_i\tilde{w}_j + w_i\tilde{w}'_j)w_k\tilde{w}_l dxdy$$

$$+ \iint_F \sum_{i=1}^{n} \sum_{j=1}^{n} c_{n,i,j} (u_x w_i' \tilde{w}_j + u_y w_i \tilde{w}_j') w_k \tilde{w}_l \, dxdy$$

$$- D \iint_F (w_\partial'' \tilde{w}_\partial + w_\partial \tilde{w}_\partial'') w_k \tilde{w}_l \, dxdy$$

$$+ \iint_F (u_x w_\partial' \tilde{w}_\partial + u_y w_\partial \tilde{w}_\partial') w_k w_l \, dxdy$$

$$=^{\dagger} \Phi \sum_{i=1}^{n} \sum_{j=1}^{n} c'_{n,i,j} \int_0^{\ell} w_j \tilde{w}_l \left( \int_0^{\ell} w_i \tilde{w}_k \, dx \right) dy$$

$$+ \sum_{i=1}^{n} \sum_{j=1}^{n} c_{n,i,j} \left\{ \int_0^{\ell} w_j \tilde{w}_l \left[ \int_0^{\ell} (D w_i' \tilde{w}_k' + u_x w_i' \tilde{w}_k) w_i w_k \, dx \right] dy \right.$$

$$\left. + \int_0^{\ell} w_i \tilde{w}_k \left[ \int_0^{\ell} (D w_j' \tilde{w}_l' + u_y w_j' \tilde{w}_l) w_j \tilde{w}_l \, dx \right] dy \right\}$$

$$+ \int_0^{\ell} w_\partial \tilde{w}_l \left[ \int_0^{\ell} (D w_\partial' \tilde{w}_k' + u_x w_\partial' \tilde{w}_k) w_i w_k \, dx \right] dy$$

$$+ \int_0^{\ell} w_\partial \tilde{w}_k \left[ \int_0^{\ell} (D w_\partial' \tilde{w}_l + u_y w_\partial' \tilde{w}_l) w_j \tilde{w}_l \, dy \right] dx$$

$$=^{\dagger\dagger} \sum_{j=1}^{n} \left\{ \int_0^{\ell} \tilde{w}_j \tilde{w}_l \, dy \cdot \left[ \Phi \sum_{i=1}^{n} c'_{n,i,j} \int_0^{\ell} w_i w_k \, dx \right. \right.$$

$$\left. + \sum_{i=1}^{n} c_{n,i,j} \left( D \int_0^{\ell} w_i' w_k' \, dx + \bar{u}_x \int_0^{\ell} w_i' w_k \, dx \right) \right] \Bigg\}$$

$$+ \sum_{i=1}^{n} \left\{ \int_0^{\ell} w_i w_k \, dx \cdot \left[ \sum_{j=1}^{n} c_{n,i,j} \left( D \int_0^{\ell} \tilde{w}_j' \tilde{w}_l' \, dy + \bar{u}_y \int_0^{\ell} \tilde{w}_j' \tilde{w}_l \, dy \right) \right] \right\}$$

$$+ \int_0^{\ell} \tilde{w}_\partial \tilde{w}_l \, dy \cdot \left( D \int_0^{\ell} w_\partial' w_k' \, dx + \bar{u}_x \int_0^{\ell} w_\partial' w_k \, dx \right)$$

$$+ \int_0^{\ell} w_\partial w_k \, dx \cdot \left( D \int_0^{\ell} \tilde{w}_\partial' \tilde{w}_l \, dy + \bar{u}_y \int_0^{\ell} \tilde{w}_\partial' \tilde{w}_l \, dy \right) \qquad \text{(C4)}$$

In this form, all of the integrals of the products of basis functions have been evaluated for the one-dimensional case.

$^{\dagger}$ with rearrangement and integration by parts

$^{\dagger\dagger}$ with velocity approximated by average velocity over the grid block